FEBS Letters

FEBS PRESS science publishing by scientists

REVIEW ARTICLE

Imaging the adenovirus infection cycle

Noémie Pied and Harald Wodrich

CNRS UMR 5234, Microbiologie Fondamentale et Pathogénicité, Université de Bordeaux, France

Correspondence
H. Wodrich, CNRS UMR 5234, Microbiologie Fondamentale et Pathogénicité, University of Bordeaux, 146 rue Léo Saignat, 33076 Bordeaux Cedex, Bordeaux, France
Tel: +33-(0)5 57 57 17 63
E-mail: harald.wodrich@u-bordeaux.fr

(Received 15 October 2019, revised 18 November 2019, accepted 20 November 2019, available online 12 December 2019)

doi:10.1002/1873-3468.13690

Edited by Urs Greber

Incoming adenoviruses seize control of cytosolic transport mechanisms to relocate their genome from the cell periphery to specialized sites in the nucleoplasm. The nucleus is the site for viral gene expression, genome replication, and the production of progeny for the next round of infection. By taking control of the cell, adenoviruses also suppress cell-autonomous immunity responses. To succeed in their production cycle, adenoviruses rely on well-coordinated steps, facilitated by interactions between viral proteins and cellular factors. Interactions between virus and host can impose remarkable morphological changes in the infected cell. Imaging adenoviruses has tremendously influenced how we delineate individual steps in the viral life cycle, because it allowed the development of specific optical markers to label these morphological changes in space and time. As technology advances, innovative imaging techniques and novel tools for specimen labeling keep uncovering previously unseen facets of adenovirus biology emphasizing why imaging adenoviruses is as attractive today as it was in the past. This review will summarize past achievements and present developments in adenovirus imaging centered on fluorescence microscopy approaches.

Keywords: adenovirus; live-cell imaging; microscopy; viral genome; virus assembly; virus egress; virus entry; virus replication; virus trafficking

Adenoviruses (Ads) are nonenveloped icosahedral viruses with a diameter of ~ 90 nm with slight structural differences between genotypes. The majority of the Ad capsid shell is composed of 240 hexon trimers, and each of the 12 vertices of the icosahedron is occupied by a penton. Pentons are involved in cell attachment and receptor recognition and are composed of the pentameric penton base from which the trimeric fiber molecule extends. Minor capsid proteins IIIa, VI, VIII, and IX are embedded in the capsid and contribute to capsid stability. Protein VI is located at the inner surface of the capsid, and biochemical data suggest that it may connect the capsid to the core containing the viral genome *via* protein V. The genome is a ~ 36-kb double-stranded linear DNA molecule with the terminal protein (TP) covalently bound to each 5′-end. Adenovirus genomes are highly condensed and organized into chromatin by several hundred copies of

Abbreviations
ADP, adenovirus death protein; Ads, adenoviruses; AFM, Atomic force microscopy; AI, artificial intelligence; AVP, adenovirus protease; CLEM, correlative light and (cryo-) electron microscopy; CRM1, chromosome maintenance 1; DBP, DNA binding protein; DDR, DNA damage response; DHM, Digital holographic microscopy; DIC, differential interference contrast; EM, electron microscopy; FISH, fluorescence *in situ* hybridization; FM, fluorescence microscopy; FP, fluorescent protein; FRAP, fluorescence recovery after photobleaching; FRET, fluorescence resonance energy transfer; HMGB, high mobility group B; IF, immunofluorescence; IFN, interferon; LMB, leptomycin B; LSCM, laser scanning confocal microscopy; LSFM, Light sheet fluorescence microscopy; MT, microtubule; MTOC, microtubule-organizing center; NES, nuclear export signals; NLS, nuclear localization signal; NPC, nuclear pore complex; PALM, photoactivated localization microscopy; PML, promyelocytic leukemia; RC, replication compartment; SMLM, Single-molecule localization microscopy; STED, Stimulated emission depletion microscopy; STORM, stochastic optical reconstruction microscopy; TIRF, Total internal reflection fluorescence; TP, terminal protein; ViPR, virus induced post replication.

the histone-like protein VII and the protamine-like basic protein X/μ-peptide. The capsid contains a small number of protein IVa2 involved in genome packaging and of the adenovirus protease (AVP) required for capsid maturation (summarized in Ref. [1]).

Adenovirus particles are not static entities, and the viral life cycle is a coordinated process of conditional steps triggered by capsid alterations. Maturation of newly assembled virions leads to the cleavage of precursor proteins IIIa, VI, VII, VIII, TP, and X to convert the capsid into a metastable entity [2]. Maturation is required for the subsequent stepwise disassembly process upon cell attachment [3]. Most fluorescence microscopy (FM) studies employed AdC2/5 in epithelial cell systems, and cumulative evidence has shown that they attach and enter cells within ~ 5 min and by ~ 15 min postinfection reach the cytosol [4–8]. It takes about ~ 30–45 min for Ads to traverse the cytosol and to accumulate at the nuclear pore complex (NPC) for nuclear genome import. At each step, the capsid undergoes structural changes until capsid disintegration at the NPC liberates the genome [6]. Gene expression starts within ~ 1–2 h postinfection with expression of the E1A protein [9]. E1A promotes S-phase progression and drives expression from the E2, E3, and E4 transcription units, which are essential to start genome replication and suppress antiviral immunity responses including apoptosis, DNA damage response (DDR) and inflammation [10–12]. Replication compartments (RC) are formed at ~ 6–8 h after initial entry and lead to dramatic morphological changes in the nucleus. Replication is required for late gene expression of most structural proteins [13] before nuclear capsid assembly, and packaging of replicated genomes gives rise to the next generation of viral particles [14]. New virions then undergo maturation by the AVP and are released from cells for the next infection round [15]. It should be noted that the indicated timing for gene expression and replication given in this review depends on the experimental conditions used in the cited references and is influenced by cell type and the amount of input virus.

Visualization of Ads is limited by their small size and requires high resolution and high signal intensities. Early images of Ads date back to the 1950s and were taken by electron microscopy (EM) of cells infected with a new viral agent [16,17]. This agent was named adenovirus after the adenoid tissue from which it was originally isolated [18]. Early time-course analysis describing Ad entry using EM has shaped our understanding of the underlying mechanisms [4]. Light microscopy and especially FM soon complemented knowledge from EM by labeling defined targets [19–22]. Fluorescent probes that label Ad particles for use in FM of living infected cells have added temporal and spatial resolution introducing dynamic aspects of Ad infection [23,24]. The detailed knowledge of the viral life cycle is the cumulative work of almost 70 years of research in the Ad field and is discussed in detail within the different chapters of this special issue. Imaging Ads complements biochemical, mutational, and structural approaches to understand how viruses take control of the host. In this review, we focus on past and present FM approaches that have helped decipher the Ad life cycle at the cellular level. Because most studies use C-type viruses, particularly AdC2 or AdC5 in epithelial cells, we will focus on this model. We start our review with a brief overview of the different labeling and detection strategies used when imaging Ads. We then discuss examples where imaging has contributed to clarify steps of the general Ad life cycle, following the sequential events from entry to egress, and provide examples where these contributions were subsequently exploited to study Ad interactions with the host. We conclude the review with a brief outlook to novel approaches and open questions.

General considerations when imaging Ad

Ad imaging with FM requires the definition of a labeling strategy, a suitable cell model, and imaging technique; all options have advantages and disadvantages. The following section provides a brief overview of the most frequently used FM approaches and labeling strategies. For more detailed reviews, the reader is referred to [25–27].

Choosing an imaging approach

Wide-field, epifluorescence microscopy is a cost-effective and robust imaging method, which has been frequently used to image Ad infection [7,28–32]. This technique allows the generation of bright signals at fast temporal resolution because the entire sample is visualized at once. To illuminate the sample, light, usually from a LED source, is filtered through an excitation filter to achieve the desired wavelength compatible with the fluorophore of choice. Emitted light from the sample then passes through an emission filter and is collected by a camera. The camera captures the entire emission signal from the whole sample including out-of-focus photons. Therefore, bright signals at fast temporal intervals can be generated at the cost of increased image noise due to scattered light (blurry images).

Total internal reflection fluorescence (TIRF) is a variation of wide-field microscopy based on the reflection of the light on coverslips, allowing excitation of

the sample via an evanescent wavelength. Only the part of the sample close to the coverslips is illuminated. This reduces photobleaching and decreases noise from out-of-focus excitation, but limits the penetration depth to ~ 100 nm. Consequently, TIRF is essentially used to image Ad processes close to the cell surface [33,34].

To overcome the problems associated with wide-field illumination, laser scanning confocal microscopy (LSCM) [35] has been used for Ad infection [36–40]. LSCM uses an excitation laser of a specific wavelength to scan a defined area of the sample, while emission light is collected through a pinhole that removes out-of-focus photons coming from the sample. This feature controls the depth of the field of view and allows collecting serial optic sections, providing improved spatial resolution and image contrast. The drawback of pinhole collection is the reduced amount of collected photons, which requires high intensity of excitation light. Slower acquisition time and higher light input can cause photobleaching and phototoxicity, which can be a major limitation when analyzing living cells, fast biological processes, or weak signals. To limit the excitation energy and increase acquisition speed, spinning disk confocal microscopy can be used. Rather than using a single pinhole, several pinholes are placed on a rotating disk allowing for multiple simultaneous scans of the entire sample, essentially keeping the technological advantages of the LSCM approach; this is especially suitable for live-cell imaging of Ads [41–43]. However, arrayed pinholes collect less light and the reduction of out-of-focus light is less efficient due to pinhole cross talk reducing the image contrast.

Techniques have been developed for LSCM such as fluorescence recovery after photobleaching (FRAP) to study protein dynamics and fluorescence resonance energy transfer (FRET) to study protein interactions [44]. FRAP uses fluorophore bleaching and fluorescence recovery as a parameter to characterize the dynamic behavior of the labeled molecule [45,46]. FRET uses the transfer of excited state energy of a donor fluorophore to an acceptor fluorophore as readout for proximity. Close proximity of donor and acceptor quenches donor fluorescence and reduces its fluorescence lifetime, while separation of the labeled partner results in fluorescence lifetime increase [8].

The diffraction limit of light restricts optical resolution to ~ 200 nm lateral and ~ 500 nm axial resolution [47], which is far above the 90 nm size of Ads. Super-resolution microscopy techniques (nanoscopy) overcome this diffraction limit pushing resolution into the nm scale. The deterministic approach uses confocal technology to precisely determine the exact spatial localization of the signal, while the stochastic approach uses wide-field technology to determine the origin of the signal. Stimulated emission depletion microscopy (STED) combines an excitation laser and a depletion laser. The depletion laser forms a geometrical pattern around the excitation laser and forces excited fluorophores back into dark state without emitting fluorescent light, essentially limiting the illuminated area at the focal point, greatly enhancing the spatial resolution at the cost of photon collection. The STED resolution limit is infinite and only determined by the laser power, but practically ~ 50 nm in lateral and ~ 150 nm in axial resolutions are routinely achieved [48]. STED remains technically challenging, and few applications for Ads exist [43,49]. Single-molecule localization microscopy uses sequential excitation and detection of a limited number of molecules over time using photoconversion of a dye attached to the specimen of interest. Single images are then processed to generate a computed probability (stochastic) image of the origin of the fluorescence. Image generation through photoactivated localization microscopy (PALM) uses dyes that are activated, detected, and bleached (single use), while stochastic optical reconstruction microscopy (STORM) uses photoswitchable dyes (multiple use) that have a dark state [50,51]. Both PALM and STORM can reach up to 20 nm in lateral and less than 50 nm in axial resolution, but require extensive, time-consuming postprocessing of individual images and so far have not been used to study Ad infection.

Labeling strategies for Ad particles or capsid components thereof

To use FM in Ad imaging, labeling strategies are crucial. Figure 1 provides an overview of the different strategies for capsid and genome labeling discussed in this section. Indirect immunofluorescence (IF) using antiserum from AdC5-inoculated rabbits paired with fluorescein-labeled secondary antibodies was the first FM strategy to stain virus-infected cells and allowed quantifying the number and timing of appearance of infected cells [20]. Subsequent studies used IF to detect Ads and adenoviral gene products even before their biological significance was fully understood, exemplified by the P-antigen [22,52] later shown to detect the single-strand DNA binding protein (DBP) [53,54], and the T-antigen [21,22] later shown to detect the transforming early E1B-55k protein [55–57]. Today, several specific antibodies for FM exist against structural and nonstructural Ad proteins, summarized in Table 1.

To study intact Ad particles such as upon entry, direct labeling of Ad capsids was developed to complement IF analysis and extend observations to living

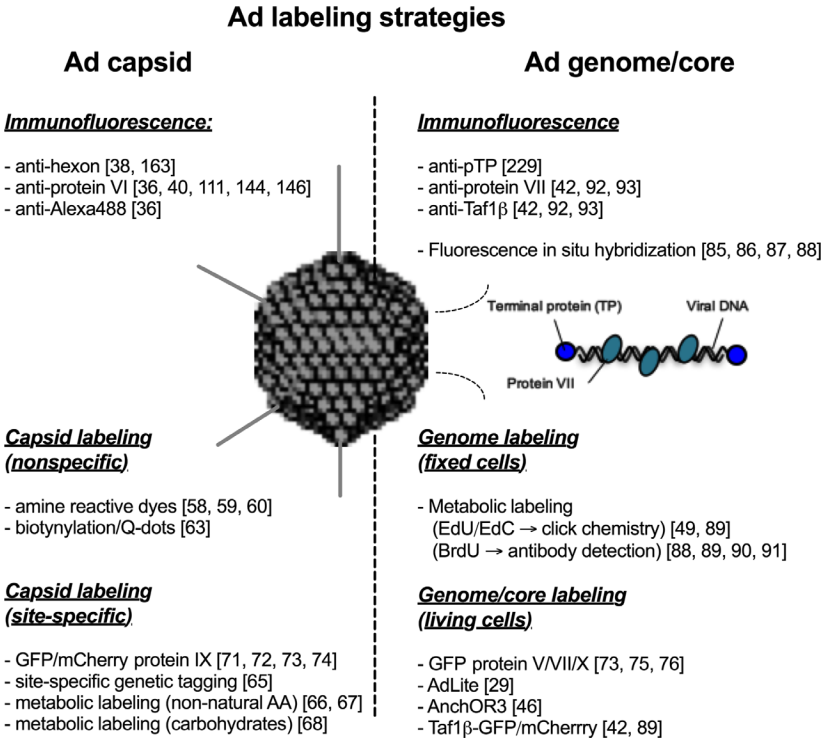

Fig. 1. Adenovirus labeling strategies. Left: Capsid labeling strategies; detection of Ad capsids in FM can be either indirect using immunofluorescence methods or through direct labeling of the whole capsid using nonspecific labeling with amine reactive dyes or site-specific incorporation of chromophore reactive groups. Right: genome labeling strategies; detection of viral genomes can be done by detecting genome-associated proteins with immunofluorescence methods or by metabolically labeling the genomes with modified nucleotides during production. Fluorescent proteins binding to the DNA or the viral core are suitable tools to detect Ad genomes in living cells (see text for details).

Table 1. Antibodies against adenoviral proteins used in fluorescence microscopy.

Structural proteins		Nonstructural proteins	
Ad protein	Reference	Ad protein	Reference
Hexon	[38]	VIa2	[326]
Hexon (R70)	[163]	DBP	[54,327]
Penton	[321,322]	preTP	[229], described in Ref. [328]
Fiber	[321]	E1A (AdC5)	[329], described in Refs [330,331]
IIIA	[323]	E1A (AdA12)	[332]
V	[260], described in Ref. [324]	E1B-55k	[57]
VI	[146]	E2-Pol	[333], described in Ref. [334], EM only
VII	[42,176,177]	E3-11.6k	[261], described in Ref. [335]
VIII	[258], western blot only	E4-ORF6	[336]
IX	[322]	E4ORF3	[337]
X	N.A.	L1-52/55k	[249]
AVP (L3-23k)	[2,325], western blot only	L4-22k	[253]

cells [23,24]. The principle is based on limited labeling of the capsid with dyes reactive to accessible primary amine groups [58–60]. This strategy is applicable to other Ad species [61] or viral proteins [62]. Alternatively, Ads have been labeled with biotin groups to couple quantum dots (Q-dots), small particles containing highly photostable inorganic dyes *via* streptavidin [63]. An ever-expanding range of dyes with different excitation properties and ready-to-use kits has made direct capsid labeling a valuable and easy-to-use approach [64]. For site-specific labeling of individual proteins on the capsid surface, reactive side groups can be introduced during virus production either genetically [65] or through metabolic labeling with unnatural amino acids [66,67], or sugars [68] followed by covalent modification with fluorophores using biocompatible click chemistry [69].

An alternative capsid tagging method is the cloning of a fluorescent protein (FP) fusion tag into the viral genome such as the enhanced GFP [70]. Enhanced GFP and variants are small, relatively inert FPs with high quantum yields, and specific excitation and emission spectra ideal for *in vivo* detection in FM. Their size (26 kDa) puts practical limitations to the amount of FP molecules that can be incorporated into Ad particles. Tagged Ad particles exploited the carboxy terminus of surface-exposed minor capsid protein IX [71–74] and the core-associated proteins V, VII, and X, either expressed from heterologous promoter [73,75] or as tagged genomic versions [76]. However, in all instances, the tag was reported to negatively

influence several parameters of viral infectivity. Many capsid tagging approaches were used for *in vivo* imaging, for example, of conditionally replicating oncolytic adenoviruses in mouse models, which is discussed elsewhere [77–84].

Direct detection of Ad genomes was initially done through different fluorescence *in situ* hybridization (FISH) techniques [85–88]. A drawback of FISH is the harsh specimen treatment to denature the DNA target. Cell-permeable labeling of viral DNA with 'clickable' nucleoside analogs such as 5-ethynyl-2′-deoxycytidine (EdC) permitted metabolic labeling of viral genomes during replication and, upon cell fixation, their detection *via* azide-modified FPs [49,89]. A widely used alternative is metabolic 5-bromo-2′-deoxyuridine (BrdU) labeling and subsequent antibody detection of BrdU incorporated into viral genomes [88–91]. Antibody detection of the genome-associated protein VII is frequently used as an indirect method for Ad genome detection. Protein VII detection results in clear punctuated signals for genomes after nuclear arrival at least during the first hours of infection [42,92,93]. Antibodies against TAF1β/SET, which associates with protein VII on incoming genomes, provide an alternative detection method for incoming genomes [42,92,93]. The ability to quantitatively bind protein VII on incoming genomes was exploited as the first robust detection system for incoming genomes in live-cell imaging by fusing TAF1β/SET with GFP or mCherry [42,89,94]. Few attempts have been made to label Ad genomes in living cells throughout the replication cycle. In the AdLite system, multiple genomic copies of the TetO repressor binding sequence were generated and viruses were grown in GFP-tagged TetR protein-expressing cells. This allowed visualizing particles during cytosolic transport upon entry, but the signal was lost during nuclear genome import [29]. *AnchOR3*-tagged Ad is the first system permitting genome detection throughout the whole replication cycle in living cells without negative impact on transcription or replication. *AnchOR3* uses genomic insertion of short repeats, based on the bacterial partitioning system [95]. The sequence promotes oligomerization of a GFP-tagged reporter protein (OR3-GFP) upon binding to double-stranded viral DNA, generating a bright fluorescent spot that marks individual incoming as well as replicated genomes [46].

Labeling strategies and use of cell models

Labeling the host cell is an important part of FM in Ad imaging. A plethora of commercial antibodies exist to detect specific proteins in cells. In addition, several specific compartment or cellular organelle markers exist and can be used to provide a reference in infected cells [25,96]. The nonexhaustive list comprises chloromethyl-X-rosamine known as MitoTracker for mitochondria [97], BODIPY or ER-Tracker for the endoplasmic reticulum [98], or LysoTracker for lysosomes [99]. pH-sensitive dyes such as fluorescein are used to monitor pH changes in the cell [100], and silicon rhodamine dyes have been used to stain actin and tubulin filaments [101]. Tagging overexpressed proteins with FP-tags is also widely used in live-cell imaging, and several companies offer a range of suitable expression vectors. To visualize endogenous proteins in living cells, FP-tagged nanobodies (chromobodies) provide several advantages. Nanobodies are the smallest antibody structure with binding capacity [102,103]. Chromobodies are expressed as FP-targeting endogenous epitopes [104] compatible with live-cell imaging and super-resolution approaches [105,106].

The vast majority of FM of Ad infection uses adherent immortalized cell culture models such as cervix carcinoma-derived HeLa or KB epithelial cells [5,7,24,37,107,108] the latter being contaminated with HeLa cells and should not be used anymore. Other cell models include lung epithelia-derived adenocarcinoma A549 cells [8,60,109] or osteosarcoma-derived U2OS epithelial cells [42,110,111]. All of these cell lines support the Ad life cycle, and their flatness and favorable nucleus-to-cytosol ratios make them ideal for FM. Ads display tropism for epithelial cells and, depending on the subgroup, may use different receptors such CAR (coxsackie and adenovirus receptor) and integrins, CD46, or sialic acids [112,113]. Functional receptor availability is important, and model cell lines may have different receptor densities [61], limiting infection efficiency [114]. For example, CAR is present on many epithelial cells, but is hardly expressed on monocyte-derived THP-1 cells [115] or alveolar macrophages [116], while in neurons, CAR holds additional functions in Ad entry [117]. Many cell lines have dysfunctional pathways affecting the Ad life cycle [118]. In contrast, adherent primary cells such as fibroblasts may retain vital signaling pathways, but are difficult to infect due to the lack of primary receptors. Restoring CAR expression in fibroblasts can circumvent this problem [119] and help identify differences to immortalized cells [39,120].

Primary immune cells such as macrophages or dendritic cells might also be employed to study Ad infection and antiviral responses. Low expression of CAR makes them difficult to infect [116], and their morphology is less convenient for imaging approaches although feasible [121–123]. Choosing an appropriate cell model for Ad imaging thus depends on a balance between

convenience of use and the biological question to be addressed.

From the cell surface to the nuclear pore

Ad infection starts with specific cell surface receptor binding on the target cell. Receptor binding triggers virus uptake by endocytic mechanisms. Endocytosed viruses undergo structural alterations and escape from the endosomal compartment by membrane lysis to enter the cytosol. Cytosolic viruses use directed microtubule transport to reach the nucleus. Docking at the NPC promotes capsid disassembly and genome import. Imaging Ad using FM methods was instrumental and provided direct evidence for many of these steps.

Cell attachment and endocytosis

Receptor binding at the cell surface was first visualized by detecting AdC5 with IF [124] or rhodamine-labeled AdC2 capsids [23]. Both studies showed that low-temperature binding results in a uniform cell surface distribution that transforms into clusters upon shifting the temperature to 37 °C in a coordinated process, which was blocked by drugs affecting the cytoskeleton. The authors concluded that Ad binding redistributes and alters mobile putative receptors in the plasma membrane conducive to virus attachment and internalization. Clustering was also observed upon AdC2 binding to HeLa cells using specific antibodies against fibronectin and vibronectin, two integrin substrates [125]. Integrins αvβ3 and αvβ5 were identified as AdC2 receptors that promote internalization through conserved RGD peptide motives in the penton base [126] followed by the identification of CAR, which is responsible for the fiber-mediated initial cell binding [127].

Atto-dye-tagged AdC2 was tracked by TIRF microscopy to investigate mobility upon cell attachment and uptake [33]. Automatic single-particle tracking and trajectory segmentation [128] distinguished diffusion, drift, and confined motions as possible particle movements. A virus internalization assay (based on dynamin-GFP intensity peaks upon Ad endocytosis) revealed that most Ads were in diffusive motion during the first 15 s of infection, and then, diffusion rates decreased whereas drifting and confined movement increased. Diffusion and drifting motions were linked to CAR binding, while integrin affinity promoted confined movement, suggestive of a model in which integrin and CAR undergo different membrane dynamics. Adenovirus binding to both receptors may impose opposing mechanical forces, which prime capsid alterations required for uptake. Capsid alterations or 'uncoating' is essential for Ad entry [6]. Shedding of fiber molecules from attached Ads prior to endocytosis [37] is likely the earliest uncoating event [33]. FRET experiments provided support for rapid and stepwise capsid uncoating during entry [8]. FRET signals were generated by random labeling of surface-exposed capsid proteins with limiting amounts of Alexa488 (donor) and Alexa594 (acceptor) fluorophores. The FRET signal was monitored during uptake, and an increase in fluorescence lifetime (spatial separation between donor and acceptor) was observed at ~ 3 min and at ~ 60 min after temperature shift to 37 °C, coinciding with biochemically estimated early fiber release and late capsid disassembly [6].

Partial capsid disassembly is linked to Ad uptake into cells. Initial studies of EM time-course analysis suggested an endo- or phagocytic uptake [4] or direct membrane penetration [129,130]. These studies concluded that Ad enters into the cytosol as an intact particle through structural alterations of the capsid. Co-uptake of cell-impermeable fluorescent dextran showed that Ads trigger endocytosis and endosome rupture resulting in cytosolic fluorescence of the co-administered dextran [5]. In a later study, fluorescent Ads and fluorescein isothiocyanate-labeled bovine serum albumin (FITC-BSA) coupled to a nuclear localization signal (used as a fluid phase marker) showed that co-internalization of macromolecules is caused by induction of macropinocytosis and lysis of the fluid phase marker-containing vacuoles. Macropinocytosis was suggested as an alternative entry pathway but is not the major route of Ad entry [131]. The endosome compartment penetrated by Ads was also studied using FM. Endocytosed fluorescent Atto565-labeled AdC2 was costained in IF with a marker for early and late endosomes. Quantification of the costain showed that Ad passes through early endosomes (positive for EEA1, GFP-tagged Rab5, and Pi3P-targeting GFP probes), but not through late endosomes (positive for Lamp1), showing that AdC2 escapes to the cytosol from an early endosomal compartment [132]. Importantly, this study used the temperature-sensitive Ad mutant AdC2*ts1* as direct experimental control. AdC2*ts1* has a hyperstable capsid and cannot penetrate the endosome [114,133] and was shown to share the early endosomal passage with the wild-type, but later colocalized with Lamp1 and was degraded by lysosomes [132].

Most Ad studies use subgroup C viruses, AdC2 or AdC5. The example of AdC2*ts1* mutant trafficking to

lysosomes demonstrates the importance of capsid alterations for the viral fate postuptake. AdB3 and AdB7, two subgroup B viruses, use different cell surface receptors [134] and, unlike AdC2 or AdC5, traffic to lysosomes as revealed by colabeling fluorescent virus particles with endocytic and lysosome markers. The investigated subgroup B viruses also do not shed fibers, do not support fluid phase uptake, and do not escape from early endosomes. Instead, they accumulate in acidic lysosomes and escape from there to the cytosol, delivering genomes to the nucleus with several hours of delay compared to subgroup C viruses, but without a reduction in efficiency as shown by time-resolved FISH analysis [114,135,136]. Quantitative IF was used to show that AdD37, a subgroup D virus, uses caveolin-1-associated and cholesterol-facilitated entry in primary fibroblasts from cornea donors. Although membrane penetration was not determined, this is yet another example for the influence of cell and genotype [137]. Taken together, FM helped reveal that Ad entry into cells is a dynamic process influenced by the fiber molecule and capsid stability.

Endosomal membrane penetration and escape

Adenovirus-induced membrane rupture during entry was suggested many years ago based on co-internalization of otherwise non-cell-permeable toxins [138,139]. Fluorescence microscopy was used to address the role of pH in this process, but delivered controversial results. Endosome acidification inhibitors (such as chloroquine and ammonium chloride) reduced FITC–dextran cytosolic localization upon Ad entry [5], and similarly, bafilomycin A-treated cells showed extended colocalization of endocytosed fluorescent dextran with co-endocytosed Cy3-labeled AdC5 over control cells, suggesting endosomal pH contributes to Ad membrane rupture [59]. Adenoviruses tagged with pH-sensitive fluorescein indicated passage through acidic environment ~ 10 min postinfection, while reaching a neutral environment at ~ 1 h postinternalization [8]. In contrast, a fluorescent assay for direct detection and distinction of cytosolic and endosomal viruses gave different results [36]. Alexa488-tagged Ad was used to infect cells, and limited permeabilization of the plasma membrane with streptolysin O allowed the detection of cytosolic, but not endosomal, viruses with anti-Alexa488 antibodies. Using bafilomycin A, niclosamide, and ammonium chloride, this assay revealed marginal effects on cytosolic delivery of viruses (including AdB3), suggesting little, if any, role for acidification [36]. It is possible that endosome acidification occurs upon Ad entry, but it has a limited impact on the capsids ability to penetrate the endosome.

Initially, the Ad membrane lytic activity was assigned to integrin binding *via* penton [140,141]. A fluorescence-based liposome rupture *in vitro* assay identified the internal capsid protein VI as Ad membrane lytic factor, acting through an N-terminal amphipathic helix [142,143]. Subsequent studies showed that protein VI becomes exposed to antibody detection upon entry (see also Fig. 2A) providing a quantifiable IF readout for capsid uncoating concomitant to membrane rupture [36,40,144]. Producing AdC2, and the AdC2*ts1* mutant, in the presence of BrdU is an alternative detection method. Similar to protein VI, genome-incorporated BrdU can be stained in IF upon entry in an uncoating-dependent manner [90].

Membrane rupture exposes luminal glycans to the cytosol, which can be visualized using internal glycan sensors, such as galectins, accumulating at the site of membrane damage. Fluorescence detection of galectins Gal3 and Gal8, initially developed for membrane lysing bacteria [145], was exploited to visualize Ad-induced membrane rupture under FM [64,110,111,146,147]. Live-cell imaging of Alexa488-labeled AdC5 showed Gal3 punctum formation ~ 15–30 min postinfection (see also Fig. 2B), whereas no puncta were found with the uncoating-defective AdC5*ts1* control. Gal3 puncta were also positive for protein VI and EEA1, suggesting endosome penetration occurs from early endosomes. Alexa488-labeled AdC5 infecting U2OS cells stably expressing Gal3 fused to mCherry revealed rapid Gal3 recruitment upon membrane lysis in living cells at or near the cell periphery, but not for AdC5*ts1* viruses [64,110,146]. Using a protein VI mutant virus (L40Q) with reduced membrane lytic activity showed reduced and delayed Gal3 recruitment [146,148]. Live-cell imaging demonstrated that capsid egress from Gal3-positive vesicles is a rapid, directional movement, suggesting a motor-driven process [110], and dynein inhibition prevented endosomal escape, but not protein VI release and membrane lysis [111], linking endosomal escape to cytosolic transport.

Time-resolved FM imaging using calcium probes and non-cell-permeable propidium iodide revealed that AdC2 causes lesions in the plasma membrane through protein VI; these changes precede endosome uptake and trigger exocytosis of a membrane repair machinery locally, such as increasing ceramide levels conducive to Ad endocytosis, while increasing protein VI membrane binding and lysis [144]. Live-cell imaging of membrane penetration revealed that membrane fragmentation

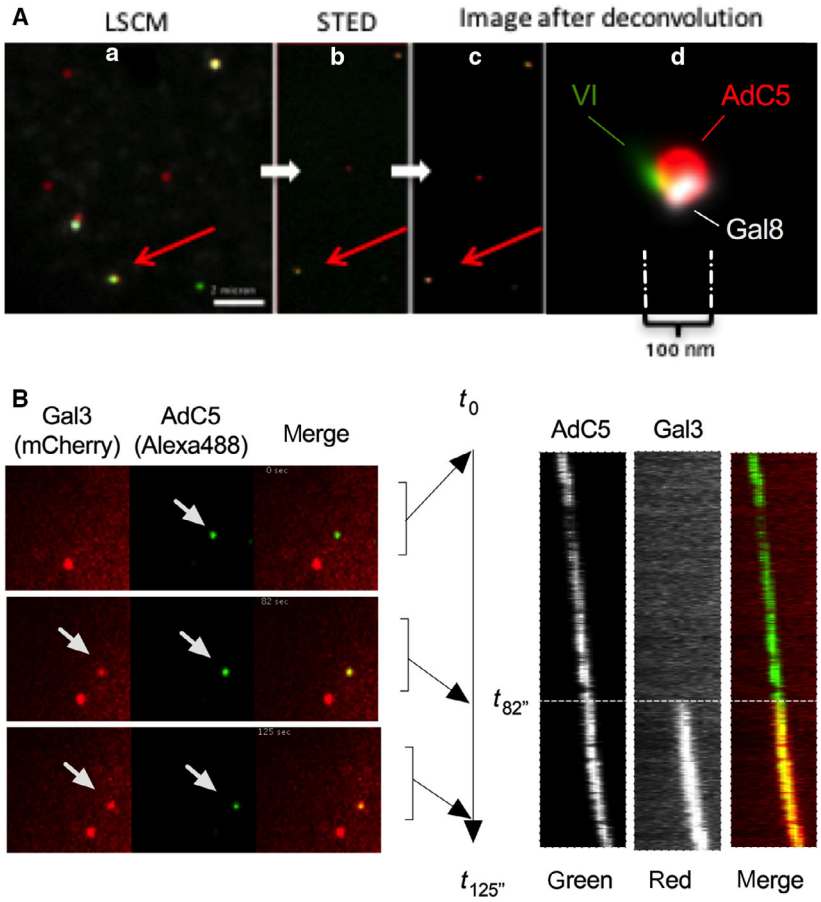

Fig. 2. Adenovirus endosome penetration: (A) Ad protein VI release. U2OS cells were infected with Alexa594-labeled AdC5 (red signal). At 20 min postinfection, cells were fixed and stained with antibodies against capsid protein VI (green signal) and galectin-8 (Gal8, gray signal). The image shows an enlarged part of the cytosol imaged by confocal microscopy (a, LSCM), super-resolution microscopy (b, STED), or following deconvolution as overview (c) or as high magnification of the particle indicated by the red arrow (d). The scale bar is 2 μm. (B) Ad endosomal membrane lysis. Gal3-mCherry-expressing U2OS cells were infected with Alexa488-labeled AdC5 and imaged by spinning disk confocal microscopy. Left: three frames of Alexa488-labeled virus particles penetrating the endosomal membrane. Arrows point at viruses inducing membrane damage visualized by Gal3 acquisition (green virus turning yellow). Right: kymograph representing the dynamic changes during endosomal membrane penetration as fluorescence intensity over time from the entire movie. The membrane lysis event is shown by appearance of Gal3 stain at 82 s (frame rate is 1 frame·s^{-1}).

and endosome escape are separate mechanistic events [64,110]. Cells respond to membrane damage in a conserved way using autophagy [149]. Time-resolved quantitative FM showed that protein VI-positive virions associate with Gal8 (and Gal3)-positive fragmented endosomes, which also stained for the autophagy marker LC3 [111,147]. Adenoviruses rapidly escaped the Gal/LC3-positive compartment, leaving protein VI behind for autophagic degradation [111,147]. Studying AdC5*ts1* in these assays confirmed that membrane damage is required for autophagy activation [111]. A second mutant, AdC5-M1, harboring a mutation in a conserved PPxY motif in protein VI, had no protein VI release or lysis defect, but was unable to escape to the cytosol and accumulated in LC3-GFP-positive autophagosomal structures, revealing that AdC5 actively suppresses the cellular autophagy response [40,111].

Adenovirus endosomal membrane penetration and escape is a prime example of how FM can visualize the profound effects of slight capsid alterations during Ad endocytic uptake. Combining quantitative FM, live-cell imaging, and mutant viruses was instrumental to separate protein VI exposure, membrane rupture, and endosomal escape of Ads at the cellular level.

Cytosolic trafficking

Rapid intracytosolic cargo transport often occurs along microtubules (MTs) using dynein motor complexes on minus-end MTs toward the nucleus or kinesin motor complexes on plus-end MTs to the cell periphery [150]. AdC2 or AdC5 was shown under EM to bind MTs in the cytosol as membrane-free particles [151,152]. Tracking Cy3-labeled Ads in live-cell imaging showed that nuclear arrival time is ~ 1 h postinfection and the maximal average velocity for AdC5 movement is ~ 0.58 μm·s^{-1}, suggesting a motor-based transport [59]. Fluorescent AdC2 infection in combination with MT-perturbing drugs and time-lapse microscopy showed that a functional MT network is necessary for rapid Ad transport [153]. Microinjection of anti-dynein antibodies confirmed a role for dynein motor complexes in minus-end movement by reducing the velocity of AdC5-Cy3 capsid [60], and dynein stimulated Ad *in vitro* binding to MT [154]. Hexon was

suggested to mediate the capsid interaction with MTs [155]. Nuclear or microtubule-organizing center (MTOC) arrival of fluorescent capsids is a convenient readout for Ad trafficking and was used to confirm a role for hexon as MT transport mediator [156,157]. The association of fluorescent capsids with dynein heavy chain after endosomal escape and until capsids reached the nucleus, but not for dynactin, confirmed that hexon serves as direct dynein receptor, supporting complementing *in vitro* studies [157]. In contrast, microinjection of anti-kinesin antibodies did not affect nuclear arrival of labeled capsids [60], while segmentation of fluorescent Ad trajectories [128] in cells overexpressing dynactin showed alteration for both plus-end and minus-end motions linking Ad to dynein- and kinesin-mediated transport [41].

Studies using fluorescent Ads showed that minus-end-directed MT movement accumulates Ads in many cells at the MTOC, suggesting that this might be an obligatory step prior to transfer toward and docking at the NPC [60,158]. Enucleated cells, where fluorescent capsids concentrate at the MTOC because the route to the nucleus is blocked, support such a model [30]. This implies that Ads at one point need to reverse directionality by either targeting plus-end MTs or different transport means. This requirement was subsequently exploited to deplete a collection of kinesins (assuming increased viral MTOC association). Indeed, depletion of kinesin-1 family member Kif5B promoted Ad MTOC accumulation, identifying a direct involvement of this kinesin in Ad transport [32]. Strong Ad MTOC accumulation also occurs when cells are treated with leptomycin B (LMB), a highly specific inhibitor of the nuclear export receptor chromosome maintenance 1 (CRM1) suggesting a role in translocating the virus to the nucleus [159]. Live-cell imaging and tracking of capsid movements showed enhanced MT association in LMB-treated cells; STED microscopy was used to plot distances between particles and MTs in the nuclear periphery and confirmed that LMB prevented virus unloading from MT [43]. However, using GFP label of the viral core (AdLite), instead of fluorescent capsids, showed no effect of MT-severing agents on intracellular mobility of the GFP signal, nucleus association, or transgene expression [29]. Also, MTOC accumulation of fluorescently labeled-AdC5 in 293 cells was shown to be MT-dependent, but subsequent genome delivery was not affected when cells were treated with MT-depolymerizing agents [160]. It remains unknown how viruses switch between plus-end and minus-end motions or whether passing through the MTOC to reach the nucleus is essential.

Docking at the NPC

Early EM images suggested Ad association with the NPC, and fluorescently labeled Ads associate with nuclei within ~ 1 h postinfection [4,59,129,151,161]. In contrast, microinjection of wheat germ agglutinin, which sterically blocks access to the NPC, or microinjection of the NPC-specific antibody RL1 prevented nuclear binding of FITC-AdC2, suggesting that NPC access is conditional for Ad nuclear attachment [6,7]. Cy3-AdC5 bound to purified nuclei from rat liver could be removed by an excess of unlabeled AdC5 and AdB7, and antibody pretreatment significantly reduced Cy3-AdC5, suggesting a direct, saturable, and specific nuclear binding [28]. AdC5 bound to the NPC in digitonin-permeabilized cells, and binding was reduced with wheat germ agglutinin or an excess of an artificial nuclear localization signal (NLS)-bearing nuclear import substrate, suggesting a functional link to nuclear import [162]. NPC docking by fluorescent AdC2 was not blocked by neither inactivation of AVP nor depletion of intraluminal calcium storage, which both affected nuclear genome import [7,133] showing functional separation of docking and genome release/import. Capsid disassembly upon NPC docking was deduced from reduced FRET signals of dually fluorescently labeled capsids observed at ~ 1 h postinfection [8] and GFP-tagged protein V-labeled AdC2 capsids losing the fluorescent signal at the NPC [76]. Adenovirus disassembly at the NPC was also shown using an anti-hexon antibody (R70) [163], recognizing an epitope hidden in intact capsids, which remained inaccessible in LMB-treated cells [159]. R70 epitope accessibility was further used to identify roles for Nup214 and histone H1 in docking and disassembly using microinjection of specific antibodies and Nup214 depletion [164,165]. Antibody detection of purified hexon binding to the nuclear rim in digitonin-permeabilized cells revealed that a small N-terminal Nup214-domain blocked both hexon binding to the nuclear envelope and Ad genome import [166]. In contrast, depletion of Nup358, another major cytosolic nucleoporin, did not prevent Ad docking or hexon binding [165,166], but was shown to limit R70 epitope accessibility, suggesting a role in capsid disassembly [165]. Disassembled AdC2 capsids (positive for R70) colocalized with several nucleoporins (Nup358, Nup214, and Nup62) at the cell periphery at ~ 3 h postinfection, indicating viral extraction of nucleoporins from the NPC, which resulted in increased permeability of the nuclear envelope for microinjected fluorescent dextrans [165]. Live-cell

imaging using photoconvertible Kaede-Nup214 confirmed that Nup214 in the cell periphery originated from the nuclear envelope and that transport required plus-end-directed partially disassembled capsid movement in association with GFP-tagged kinesin light chain 1, suggesting a role of MT linked kinesin-1 motors in capsid disassembly and genome release at the NPC [165].

From genome import to particle egress

Ad genome release and import into the nucleus

Fluorescence microscopy and EM show that Ads reach the NPC as partially disassembled, but morphologically intact particles. Although docking increases nuclear envelope permeability (shown by influx of large fluorophores [46,165]), Ad capsids do not venture beyond this point because they exceed the size limit of ~ 40 nm for nuclear import substrates [167]. Adenoviruses rather disassemble and release their highly compacted genome for nuclear import. To study genome import by FM requires capsid-independent genome detection methods (examples for Ad genome detection using FM are shown in Fig. 3). The first visualization of genomes in the nucleus used radioactively labeled AdA12 genomes in HEK cells, and discrete nuclear puncta [168,169] accumulating within 1–2 h postinfection were observed [161,169]. Developing FISH to replace radioactive methods was done to detect AdC5 genomes in infected cells [170] or biotinylated probes detectable by IF [87]. Adenovirus genome detection through FISH was used to confirm genome import through the NPC [7], to compare genome nuclear import efficiencies between Ad and artificial liposomes [171] and to identify a region in Nup214 for capsid docking [166]. FISH was also used to functionally investigate AdC5 genome import in digitonin-permeabilized cells, showing that genome import depends on energy, cellular factors, and the NPC [162] and could be outcompeted by an excess of the importin α/β substrate BSA-NLS [162], or the transportin substrate GST-M9 [172]. The exact genome import mechanism remains unclear, but may involve importing genome-associated core proteins [172–174].

Immunofluorescence detection of genome-associated protein VII is a robust alternative to detect imported genomes. Protein VII is the most abundant genome-associated protein, and protein VII epitopes are only revealed when the genome is imported into the nucleus [7]. The high local protein VII concentration on the genome provides a strong and distinguishable dot-like signal each corresponding to one viral genome, allowing quantitative assays [175]. Several protein VII antibodies have been used in IF [42,176,177].

Metabolically labeling DNA with 'clickable' nucleoside analogs was recently used to visualize incoming viral genomes with high spatial precision using STED microscopy. Unlike FISH, this method can be combined with IF. AdC5 with EdA/EdC-labeled genome showed that ~ 30 min postinfection, genomes are accessible to Alexa594-azide click detection, but are still in capsids as revealed by anti-hexon stain. Remarkably, at ~ 150 min postinfection only < 50% of genomes were imported while a significant proportion was found capsid- and protein VII-free in the cytosol, which had not been observed previously [49]. Click chemistry also showed that most (but not all) nuclear protein VII dots contain viral genomes [49]. Quantifying protein VII dots over time to determine postnuclear import is controversial. Most studies show protein VII dots for at least 10 h with progressive and transcription-dependent removal [92,93], while others suggested that protein VII is lost progressively after nuclear arrival [178] (reviewed in Ref. [179]). Thus, visualization of protein VII is a convenient surrogate marker for imported viral genomes, but should be carefully evaluated. SET1/TAF-Iβ is involved in chromatin reorganization and binds directly to protein VII [42,92,176,180]. This feature of SET1/TAF-Iβ was exploited for live-cell imaging of single incoming viral genomes and their movement in the nucleus of living cells. Stable overexpression of fluorescently labeled SET1/TAF-Iβ accumulates on incoming AdC5 genomes detectable as individual fluorescent spots. Spot tracking revealed a confined mobility upon nuclear import [42] reminiscent of anchoring to an unspecified nuclear matrix [181].

More recently, *Anch*OR3, a novel *in vivo* DNA tagging system [95], was transferred to AdC5 genomes [46]. *Anch*OR3 spots appear ~ 1 to 3 h postinfection inside the nuclei and can be traced with excellent spatial and temporal resolution and high signal-to-noise ratio. The approach was used to show association of individual AdC5 genomes with condensed chromosomes marked with fluorescently labeled histones during cell division providing a rational for genome cell-to-cell transfer in dividing cells [46].

AdV genome transcription and RNA export

Adenovirus gene expression is initiated at ~ 1–2 h postinfection from early transcription units E1-E4 and following replication at ~ 6–8 h postinfection from late transcription units L1-L5 [182–188]. Despite

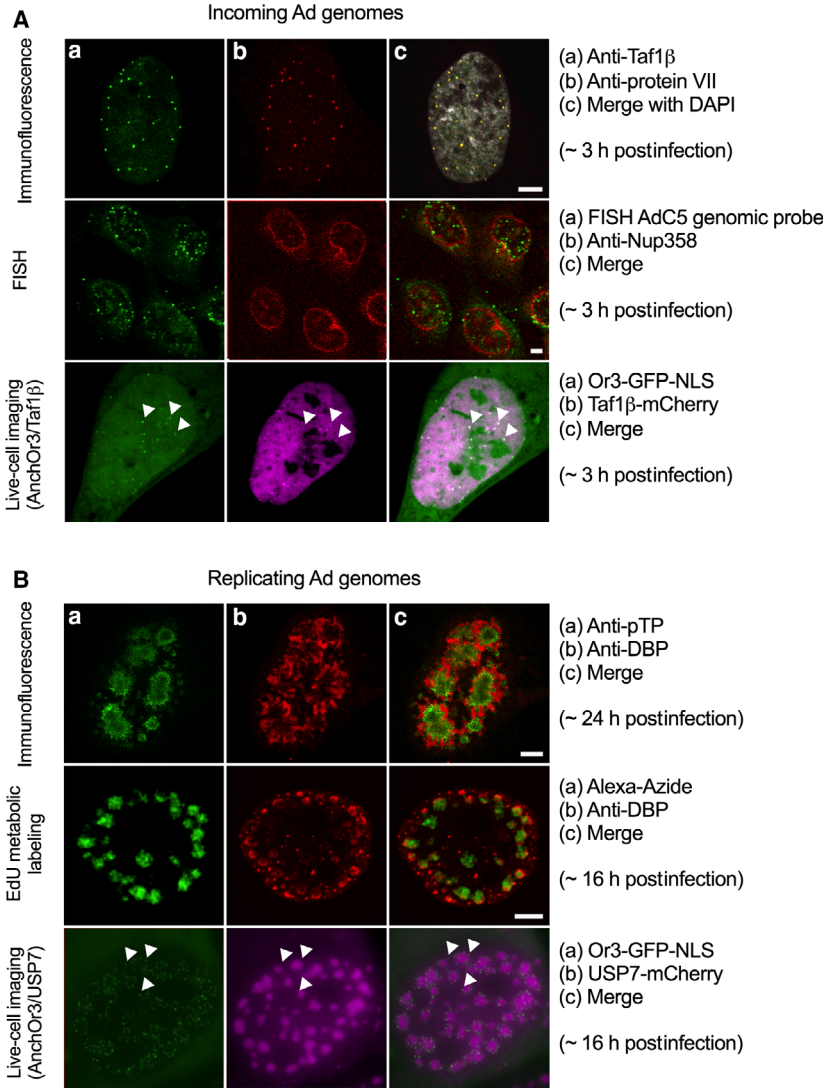

Fig. 3. Examples for adenovirus genome labeling. (A) Detection of incoming Ad genomes. Top row: U2OS cells were infected with AdC5 using 3000 particles per cell. At 3 h postinfection, cells were fixed, extracted, and stained with antibodies against endogenous Taf1β (a, green signal) and protein VII (b, red signal) colocalizing in the merge (c, DAPI stain indicates the nucleus). Middle row: HeLa cells were infected with AdC5 using 3000 particles per cell. At 3 h postinfection, cells were fixed and hybridized with a probe against the whole AdC5 genome (a, green signal). The sample was subsequently stained with antibodies against the nucleoporin Nup358 to show the nuclear boundaries (b, red signal), and both signals were combined (c). Bottom row: Or3-GFP (a, green signal) was used to transfect stable Taf1β-mCherry-expressing U2OS cells and infected with AnchOR3-AdC5 using 5000 particles per cell. The images are individual frames from spinning disk confocal live-cell imaging (merge in c). (B) Detection of replicated Ad genomes. Top row: U2OS cells were infected with AdC5 using 3000 particles per cell for 3 h followed by inoculum removal. At 24 h postinfection, cells were fixed and stained with antibodies against preterminal protein (pTP) (a, green signal) and DBP (b, red signal), and both signals were combined (c). Middle row: U2OS cells were infected with AdC5 as above. At 15 h postinfection, cells were labeled for 1 h with EdU and genome-incorporated EdU was detected with Alexa-azide (a, green signal) and stained with antibodies against DBP (b, red signal), and both signals were combined (c). Bottom row: Stable USP7-mCherry-expressing U2OS cells were infected with a mixture of 5000 particles per cell of AnchOR3-AdC5 and 500 particles of replication-competent AdC5 for 3 h followed by inoculum removal. The images are individual frames from spinning disk confocal live-cell imaging taken at ~ 16 h postinfection (merge in c). Scale bars in all images are 5 μm.

progress in visualizing incoming genomes, few attempts have been made to visualize the transcription process that follows by using FM. Most studies concern transcription and RNA processing of late gene expression and use indirect readouts. Autoradiography detecting newly synthesized RNAs and *in situ* hybridization with sequence-specific probes were used in EM to detect viral late RNAs [189,190] and PolIII

transcribed virus-associated RNAs [191]. Late viral RNAs located with early RCs suggesting a link between replication and transcription. An RNA-FISH approach with a whole-genomic AdC2 probe under nondenaturing conditions showed discrete, individual, dot-like localization of transcripts from ~ 7 to 10 h postinfection, which enlarged to ringlike structures, eventually occupying the nucleoplasm, and later at 24 h postinfection, viral RNAs were also found in the cytoplasm [192]. Specific probes overlapping the first splice junction of the tripartite leader RNA, derived from the major late promoter, detected spliced and unspliced viral mRNAs with RC suggesting cotranscriptional mRNA processing [193]. Selective DNase and RNase digestion and pulse-chase labeling of replicating genomes with BrdU followed by FISH and antibody detection revealed that freshly synthesized viral genomes spread from RCs to the surrounding nucleoplasm. Here, they serve as transcription templates providing evidence for a spatial and functional separation of replication and transcription [88]. Immunofluorescence studies complemented FISH analysis to detect the redistribution of splice and RNA processing factors confirming spatial and temporal coordination of transcription and RNA processing in the vicinity of RCs [192,194–197]. Padlock probes hybridizing with 5′ and 3′ target sequences were recently introduced to detect simultaneously AdC5 RNA and DNA at the single-cell level [198]. Padlock probes circularize upon target hybridization, and rolling circle amplification ensures strong and highly specific signals. To distinguish between RNA and DNA, exon–exon junctions have been targeted. This approach is also capable of distinguishing, for example, E1A splice variants 13S and 12S [199,200]. *A priori*, this technique permits single RNA and DNA molecule detection, but E1A transcripts were not detected before 13h postinfection, suggesting some limits to the system [198].

Interestingly, no method has been reported that accurately detects single and specific Ad RNA molecules to show their spatial and temporal organization, for example, during early transcription or RNA export, although such single mRNA detection methods for fixed and living cells exist [201–207]. Early reports showed that late in infection, export of most cellular mRNAs is inhibited in favor of viral mRNA export [208–210]. This selective viral mRNA export is mediated by a complex between the E1B-55kDa protein (E1B-55k) and E4-34kDa (E4-ORF6) localized at the periphery of RCs [211–213]. Exploiting the potential for spatial detection between nucleus and cytosol, a combination of mutational approaches, heterokaryon assays, and microinjection of purified recombinant proteins showed that the E1B-55k–E4orf6 complex constantly shuttles between the nucleus and the cytosol through nuclear export signals (NES) encoded in both proteins [214,215]. NES have been implicated in the export of some mRNAs *via* CRM1, but late viral gene expression was not sensitive to LMB, a specific inhibitor of the NES-mediated export pathway [216,217]. Instead, siRNA depletion or dominant negative mutants of the mRNA export receptor Nfx1/Tap, which colocalizes with the E1B-55k–E4orf6 complex at the RCs, were shown to reduce late viral gene expression independent of CRM1 [218]. In contrast, LMB reduced early gene expression, suggesting CRM1 supported early mRNA export [219]. Today, it remains elusive how Ads manage to specifically export their RNAs. All current studies on Ad RNA export use viral gene expression or indirect quantification methods. Direct imaging of viral mRNAs may provide great potential to solve this open question.

Ad genome replication

A serum (termed P-antigen) generated by injection of a rabbit with clarified lysates from Ad-infected cells detected nuclear dots as early as 6–7 h postinfection in HEK cells, and these dots developed into ringlike structures accurately depicting the formation of RCs during Ad replication [22,52]. The P-antigen was later shown to detect the single-strand DBP [53,54], which binds viral ssDNA during genome replication [220,221]. FISH detection of Ad genomes with rhodamine-marked RNA probes was developed to complement radioactive hybridization probes [170,222,223]. The FISH signal identified nuclear RCs with distinct morphologies that costained for DBP formally linking both markers [224]. Several studies have described how the DBP IF stain changes during Ad replication reflecting morphological changes in the nucleus. In most cells, the DBP signal is detectable at ~ 6–7 h postinfection as faint cytosolic stain translocating into the nucleoplasm by ~ 10–12 h postinfection where it eventually forms dots that fuse and grow into ringlike or globular structures morphing into larger, irregular-shaped intranuclear domains [54,224,225]. Currently, DBP is frequently used as reference stain to describe spatial and temporal events in the nucleus of Ad-infected cells [88,195–197]. In addition, DBP was used to characterize Ad replication itself [46,89,226–228] to identify cellular and viral proteins that are sequestered into viral RCs [94,229–232] or used as spatial or timing reference to study non-RC-linked events [233–236]. Recent super-resolution microscopy performed on

isolated replication compartments from infected HeLa cells suggests a dynamic RC subcompartmentalization of DBP [237]. Ubiquitin specific protease 7 (USP7/HAUSP) is a cellular protein that is functionally required for AdC5 replication [231] and phenocopies the distribution of DBP, serving as a robust alternative marker for Ad replication [89,231]. Pulse-chase experiments with BrdU incorporating genomes were used to label replication dynamics, showing the spatial separation of replication and transcription [88]. Pulse-chase labeling with EdU and click chemistry confirmed the intranuclear transport of freshly replicated genomes toward the periphery of RCs at ~ 16–20 h postinfection. In contrast, at ~ 20–24 h postinfection replicated genomes accumulated in a novel nuclear structure, which the authors termed ViPR bodies for virus-induced postreplication bodies [89], which resemble nuclear domains containing viral genomes identified by radioactive hybridization [222,223]. Virus-induced postreplication bodies were shown to be delineated by USP7 [89] and DBP [236] concomitantly with their appearance suggesting a change in replication mode. Immunofluorescence staining showed that ViPR bodies accumulate several nucleolar proteins such as Myb-binding protein 1A (Mybbp1A) [89], nucleophosmin (NPM1/B23), nucleolin (NCL), and nucleolar transcription factor 1 (UBF1) [236], previously shown to be involved in genome processing [238–242]. Because ViPR bodies contain viral chromatin and chromatin modulators, but are devoid of histones, it was suggested that they are sites of late viral chromatin assembly [46,89,236]. AdC5-labeled with *Anch*OR3 technology were used to infect U2OS cells stably expressing USP7-mCherry as RC marker allowing the first dynamic description of viral replication [46]. Quantification of the USP7-mCherry signal (RC) and the OR3-GFP signal (replicated double-stranded genomes) at high temporal resolution (20 min per frame) allowed the quantification of replication rates from the GFP signal. Early RCs coincided with replication rates of ~10 genomes per hour and genomes accumulating in their periphery. With the appearance of late RCs, replication rates suddenly increased to > 100 genomes per hour and newly synthesized genomes progressively accumulated in ViPR bodies [46]. This first dynamic description of the genome replication cycle confirmed many of the previous morphological observations done with DBP (see above), putting them into a dynamic context. The fact that genome replication has two clearly distinguishable kinetic phases was previously unknown and showed the importance of generating imaging systems for Ad that capture dynamic processes [46].

Ad assembly and egress

Adenovirus assembly generates initially immature non-infectious particles. Maturation into infectious particles involves processing of several capsid proteins by AVP [15,91,243]. Nuclear assembly was suspected following EM observation of arrays of viruses inside the nucleus of infected HeLa cells [16,17,244]. Electron microscopy also showed a paracrystalline nuclear structure not containing virus particles, but reacting with capsid specific or core specific antibodies, suggesting they could be sites of virus assembly [245,246]. Adenovirus assembly and egress is still enigmatic, and very few studies have used FM to visualize the process at the cellular level. Based on biochemical data, the use of temperature-sensitive Ad mutants, and EM analysis of purified virus intermediates, virus assembly was proposed to occur either sequentially (capsid assembly precedes genome packaging) or concomitantly (capsids and genomes assemble together) [247]. Virus assembly depends on functional viral scaffold L1-52/55k protein present in assembly intermediates, but absent from mature virions [248]. Immunofluorescence of L1-52/55k showed a nuclear distribution distinct from DBP-positive RCs suggesting spatial separation of replication and assembly [248,249], although biochemical analysis suggested that assembly requires replication [250]. A combination of IF with immuno-EM compared wild-type AdC5 with a packaging delayed mutant. BrdU-labeled freshly replicated genomes were shown to partially overlap with L1-52/55k at the periphery of RCs. Using careful EM analysis, the authors find capsids with partly inserted cores in this zone in strong support of a concomitant assembly model and propose that L1 present on assembled cores as well as immature particles drives the coupled encapsidation–assembly process [91]. Indeed, L1-52/55k also associates with protein IVa2 [251] and forms a complex with L4-22k protein that is involved in genome binding and packaging [252–254]. Alternatively, genomes may be inserted into preassembled capsids by virtue of a putative portal protein [255,256]. FM showed that protein IVa2 and DBP partially overlap in transfected cells with another assembly factor, the L4-33k protein and E4-ORF6, and all four are found by immune-EM at a single virus vertex of purified particles [256,257].

Nucleophosmin (NPM1/B23) is one of the few cellular factors for which FM suggests a role in capsid assembly. Depletion of NPM1/B23 prevents capsid assembly without affecting replication [241], and NPM1/B23 relocalizes from nucleoli in infected cells to colocalize with capsid protein IX and core protein V

and associates with empty capsids [242]. In addition, NPM1/B23 was found in ViPR bodies colocalizing with protein IVa2, suggesting a potential role in core assembly [236]. Interestingly, AdC5 lacking protein VII had no assembly default, ruling out that the major core protein drives assembly [258]. Adenovirus assembly seems to rely on cellular and viral nonstructural and structural proteins. Structural proteins have to be imported into the nucleus in large quantities using NLSs [174,259,260]. Cytoplasmic microinjection of fluorescently labeled purified hexon from AdC5 and transient expression of hexon showed that hexon nuclear import required binding to capsid protein VI. Mutational analysis and heterokaryon assays revealed import and export signals at the C terminus of protein VI providing shuttling capacity as selective hexon import adapter. C-terminal processing of protein VI by AVP late in infection removes the transport signal and increases hexon binding affinity, and the released peptide stimulates AVP driving the equilibrium toward assembly [15,62]. Nuclear import thus may be intricately linked to assembly. Adenovirus egress from the nucleus is also poorly characterized by FM. Instead, indirect measures quantifying released particles and plaque sizes are used. The E3-11.6k protein, also known as adenovirus death protein, modulates Ad egress. E3-11.6k is a glycoprotein expressed from the E3 region of AdC2 and AdC5. Early in infection, IF of infected cells shows ER/Golgi localization for E3-11.6k, while late in infection, its production picks up, and it is found predominantly at the nuclear envelope. This redistribution is correlated with efficient cell lysis resembling apoptosis [261]. Autophagy is an inducible cellular degradation pathway, and autophagy induction *via* LC3 punctum formation was observed late in AdC5-infected LC3-GFP-transfected A549 cells. In contrast, pharmacological autophagy suppression reduced particle release and late gene expression so that the precise role for autophagy in Ad release remains unresolved [262,263]. A limitation for imaging Ad egress is the lack of tools that can clearly discriminate or track newly assembled particles.

Imaging anti-adenoviral immunity

Adenoviruses that enter cells are faced almost immediately with cell intrinsic immunity mechanisms trying to sense and initiate danger signals ultimately eliminating the invader through direct degradation and by initiating a signaling cascade that activates other branches of the immune system. Those particles that manage to reach the nucleus and deliver their genomes are faced with a second wave of nuclear defense mechanisms aimed at suppressing viral gene expression and replication. Most studies on Ad-induced immunity use indirect readouts such as interferon (IFN) or NF-κB signaling, caspase activation or IL-1β secretion, or the quantification of replication, gene expression, or particle production. Increasingly, though, FM is used to support findings by providing spatiotemporal context in immune and nonimmune cells as shown by the nonexhaustive examples listed in this section.

Cytosolic antiviral immunity

Adenovirus genomes are a major pathogen pattern that can be recognized during the cytosolic passage upon entry. One of the many sensors recognizing nonmethylated (i.e., viral) DNA is Toll-like receptor 9 (TLR9), located in the endosomal compartment, triggering IFN signaling *via* MyD88 [264]. Costaining with TLR9 in breast cancer stem cells infected with a conditional replicating oncolytic AdC5/3-D24 showed that incoming particles rapidly associate with TLR9-positive vesicles [265]. Toll-like receptor 9-independent Ad genome sensing was proposed in nonimmune cells based on IRF3-mediated IFN signaling in response to cytosolic Ad genome sensing *via* cGAS/STING/TBK1 [266–268], a pathway also active in macrophages [268,269]. How and when capsid-protected cytosolic Ad genomes are sensed is less clear. FM detection of metabolically labeled genomes revealed cytosolic misdelivery of a large proportion of viral genomes at the nuclear pore potentially serving as substrate for cGAS/STING sensing [49]. Antibody-opsonized (immune-complexed) AdC5 (IC-AdC5) colocalized upon uptake into HeLa cells with TRIM21, and this led to the ubiquitination of the viral capsid. As a consequence, viral capsids are degraded in a TRIM21-dependent process reducing infection [270,271]. Genome labeling with BrdU revealed cytosolic genome exposure upon TRIM21-mediated degradation which colocalized with cGAS, supporting a model for initial TRIM21-mediated sensing and processing of IC-AdC5 to expose secondary epitopes, that is, viral genomes for downstream sensors like cGAS and RIG-I [272]. Immune-complexed AdC5 also induced DNA-sensing AIM2 inflammasome (absent in melanoma 2) activation in monocyte-derived DC (MoDC). Fluorescently labeled IC-AdC5 (but not AdC5 alone) contained in TLR9-positive MoDC endosome was shown by IF to release protein VI and to accumulate Gal3 and P62 indicating membrane rupture, which activated the AIM2 inflammasome shown by colocalization of Ad capsid with AIM-2 and ASC and functional assays [122]. Like for the TRIM21 example above, IC-AdC5 triggers capsid

disassembly provoking membrane rupture and cytosolic activation of a genome sensor [122]. AdC5 infection of differentiated THP-1 cells activates the NLRP3 inflammasome resulting in the release of large amounts of cathepsin B into the cytosol in wild-type, but not in membrane lysis-impaired AdC5*ts1*-infected cells, supporting a direct link to membrane damage [273]. AdC5-induced membrane damage activates antiviral autophagy in nonimmune cells. Immunofluorescence and live-cell imaging showed that (protein VI-positive) virions in the process of endosome penetration associate with Gal8 (and Gal3)-positive fragmented endosomes, which also accumulated ubiquitin and several autophagy factors (e.g., LC3, NDP52, P62) resulting in autophagy activation [111]. The data support a model that rapid endosomal escape and suppression of autophagy through capsid-mediated processes are key elements of AdC5 entry to evade antiviral autophagy in response to membrane damage [111]. Imaging antiviral immunity also captured the absence of membrane damage. Defensins [90,274] and complement factor C4 [275] are two soluble extracellular antimicrobial molecules that bind and neutralize AdC5. Immunofluorescence analysis showed that entering capsids opsonized with either molecule failed to release protein VI, did not trigger Gal3 puncta nor exposed BrdU-labeled genomes in support of a capsid stabilizing phenotype, which prevents endosome penetration. Instead, capsids remained endosomal and accumulated in lysosomes [90,274,275]. Taken together, these studies provide several FM examples of cytosolic antiviral immunity, showing how detecting protein VI upon entry as membrane penetration marker [40] helped define a spatial and functional readout to characterize the cellular response to Ad invasion.

Nuclear antiviral immunity

Having lost their protective capsid, imported Ad genomes are particularly vulnerable to nuclear pathogen sensor and effector molecules before viral gene expression. Still, live-cell imaging of incoming AdC5 genomes suggests protection from early recognition by several known antiviral sensors and effectors, including promyelocytic leukemia (PML) nuclear bodies (PML-NBs) which target several nuclear replicating viruses [276–281]. DNA FISH to detect incoming AdC5 showed that most genomes localized adjacent to PML-NB at 4 h postinfection, but not at 1.5 h postinfection [282]. Detailed IF and live-cell imaging showed that this early association with PML-NBs is not an intrinsic property of the incoming genome, nor is it imposed by PML-NBs or its constituents, but may depend on DBP [280]. At ~ 6–8 h postinfection, AdC5 dramatically alters the organization of PML-NBs and reorganizes them into stable track-like structures, for example, as shown for PML and SP100 in HeLa cells [283,284]. BrdU labeling and detection of splice proteins showed that early PML tracks are not replication sites [283], although at ~ 12–16 h postinfection, SP100 accumulates in DBP-positive RCs [233]. Overexpression of PML in HeLa cells or treatment with IFN to stimulate PML-NB protein expression delayed replication suggesting Ad counter regulation [233]. Reorganization of PML was attributed to Ad-encoded E4-ORF3 and E1B-55k proteins. Experiments using IF showed that E4-ORF3 colocalizes with PML, and deletion of E4-ORF3 in AdC5 prevented PML track formation [283]. Track formation is an intrinsic property of E4-ORF3 linked to a C-terminal oligomerization domain [285]. Moreover, E4-ORF3 forms a complex with E1B-55k and both proteins localize to PML tracks in AdC5-infected HeLa cells or when overexpressed individually [286]. The biological significance of PML track formation is not completely clear, but the ability of E4-ORF3 to induce tracks correlates with its ability to overcome replication restriction by IFN shown with DBP stain in fibroblast and Vero cells and is conserved between different serotypes [287]. Independent reports show that protein IX and protein VI also reorganize PML-NBs, although the biological significance is not yet clear [288,289].

The DDR mediated by the MRN (Mre11, Rad50, Nbs1) complex also targets invading and replicating Ad genomes [290]. In AdC5-infected HeLa cells, Mre11 and Nbs1 were found in foci close to RCs and Mre11 levels were reduced compared to uninfected cells. When an E4-deleted AdC5 was used, MRN colocalized with RCs and BrdU-labeled genomes and replicated genomes formed concatamers demonstrating cellular repair of 'damaged' genomes. Viral deletion mutants and individually expressed proteins further showed that E4-ORF6/E1B-55k is important for MRN complex degradation, while E4-ORF3 redistributes MRN into PML tracks [290,291]. Mre11, Rad50, and Nbs1 relocalization *via* AdC5 E4-ORF3 also promotes genome replication [291] and is required to target the MRN complex into cytosolic aggresomes [292]. In contrast, E4-ORF3 from AdE4 or AdA12 did not displace Nbs1 from RCs indicating genotype differences [292]. In infected cells, E4-ORF6/E1B-55k associates with cullin5, elongins B and D, and Rbx to form a E3 ubiquitin ligase [293,294] able to target the MNR complex for proteasomal degradation [290]. The E4-ORF6/E1B-55k ligase complex shuttles between the nucleus and cytoplasm, and subcellular localization of

substrates (i.e., p53 and Nbs1) was exploited to identify functional domains in E1B-55k for substrate recognition and targeting [295]. These examples show how differences in subcellular localization contributed to characterize E4-ORF3 and the E4-ORF6/E1B-55k ligase complex, identifying them as potent viral countermeasures in the fight against PML-NB and DDR. However, freshly imported Ad genomes do not possess access to these proteins yet. The MRN complex recognizes double-strand breaks and induces activation of the cellular repair protein kinase ATM (ataxia telangiectasia and Rd3 related) by trans-autophosphorylation (pATM) and phosphorylation of histone variant H2AX (γH2AX). Consequently, pATM and γH2AX have been exploited as imaging markers for DDR activation. Using mutated and EdU-metabolically labeled AdC5 (e.g., E4-ORF6/E4-ORF3 double mutant or E4-deleted viruses) showed that incoming genomes activate MRN and that this response is initially suppressed by genome-associated protein VII [296]. The authors used EdU and protein VII antibodies to detect genomes and antibodies against pATM and γH2AX to stain for activation of the MRN complex and were able to show that in the absence of E4 proteins, imported genomes progressively accumulate pATM/γH2AX upon protein VII removal [296]. pATM/γH2AX marks on viral genomes were later shown to identify virus-specific DDR discriminating viral genomes from cellular damage [297]. More recently, it was shown that SET/TAF1-β recruitment to incoming genomes *via* protein VII is crucial to suppress MRN because SET/TAF1-β depletion promoted pATM and γH2AX accumulation also on protein VII-positive incoming genomes. This suggests a key role for SET/TAF1-β in DDR suppression before viral gene expression gives Ad access to a wider repertoire of instruments [298] and is a nice example how FM detection of viral substrates (i.e., the incoming genome) provides clues to understand the spatial and temporal organization of cellular response and viral countermeasure. Immunofluorescence and FRAP mobility analysis showed that protein VII also mediates retention of high mobility group B family proteins by associating with compacted cellular chromatin late in infection to counteract their release as alarmins [45]. Subcellular sequestration/degradation of cellular factors, which can easily be revealed by FM, seems to be a general way for Ad to control cell responses. For example, to control the IFN response, Ad modulates the distribution of signal transducer and activator of transcription 1 (STAT1), a major driver of the IFN response. Immunofluorescence showed that HeLa cells expressing E1A do not translocate STAT1 to the nucleus after IFN stimulation [299] and AdC5-infected cells sequester phosphorylated STAT1 in DBP-positive RCs [300].

Novel approaches

Both FM and EM have been used to investigate Ad infection [301], but never in the same sample. Correlative light and (cryo-)electron microscopy (CLEM)/cryo-CLEM combines both technologies by using EM on a fluorescent sample for high structural resolution and precise identification of specific elements in the cellular context. Correlative light and electron microscopy has been successfully applied to other viruses in entry [302], replication [303], and release [304] from infected cells (for a review, see Ref. [305]). Correlative light and electron microscopy was further used to visualize the nuclear track network formed by E4-ORF3 in AdC5-infected U2OS cells using photo-oxidation of diaminobenzidine (DAB) into a polymer that can be stained by osmium tetroxide [306]. A major hurdle that remains in CLEM is the correlation of FM and EM signals. During cryo-CLEM, the biological sample is fixed by rapid vitrification. Alexa488-labeled AdC5 infecting U2OS cells was used as readout to measure automatic FM–EM alignment showing a correlation of ~ 100 nm between FM and EM images. The resulting high-resolution image identified by the fluorescent signal showed an Ad particle in an endosome in its native state describing the first experimental cryo-CLEM pipeline for Ads inside cells [307]. Cryo-fixation and subsequent cryo-CLEM or even cryo-tomography were applied to other viruses [308,309], highlighting the enormous potential for Ad imaging as it allows the correlation of dynamic processes with ultrastructure in a native context.

Labeling strategies and bio-dyes visualize dynamic processes that can be captured by FM. However, labeling strategies remain invasive and modify the specimen. Light microscopy using phase contrast and differential interference contrast is a label-free imaging method, although with limited resolution. Digital holographic microscopy (DHM) improves acquisition of samples in phase contrast by combining a laser beam passing through the sample with a reference beam to generate a digital interference image (hologram). Using a specific algorithm, the hologram is used to digitally compute an image of the sample allowing nanoscale resolution and long-term acquisitions without focal or bleach concerns. DHM was first used to visualize cell modification, motility, and proliferation [310] and more recently applied to study cytopathic effects during viral infections [311].

Atomic force microscopy (AFM) provides nanoscale information of the surface topography of a sample, that is, an Ad particle. AFM uses a microcantilever with a tip scanning the sample surface thereby deflecting a laser beam. The modified laser beam is converted into a topological map of the scanned object. AFM can also be used for mechanistic measures such as elasticity, pressure, or compaction by applying force on the sample resulting in changes in topology. Such nano-indentation assays were used on AdC5 with the fiber of AdB35 to measure capsid stability in the presence of integrin or defensins (showing increased susceptibility or resistance to disassembly [312]) or compare stability between wild-type and AdC2*ts1* viruses (revealing different energy requirements in disassembly) [313]. Using a combination of AFM (to measure capsid stability) and TIRF (to visualize exposed viral genomes with a DNA intercalating fluorescent dye) revealed rapid genome decondensation upon capsid release [34], while AdC2*ts1* genomes are more compacted, suggesting that maturation induces viral chromatin relaxation inside the capsid and primes them for entry and disassembly [314], showing how AFM complements other Ad imaging approaches by providing biophysical information.

Light sheet fluorescence microscopy (LSFM) is a conceptually novel imaging approach based on the use of two objectives, one for illumination and one for detection positioned at a 90° angle. Compared to confocal microscopy using scanning point illumination, LSFM illuminates a complete focal plan visualizing the sample at once. This minimizes exposure time and phototoxicity and enables high frame rates for a prolonged time. The perpendicular illumination also allows the acquisition of depth in samples for adaptation to more complex, physiologically relevant models such as organs, tissue, and other 3D cultures. LSFM has not been used for Ads, but several LSFM approaches are in development and will provide revolutionary insight into dynamic processes [315,316].

Automatization, machine learning, and artificial intelligence are rapidly evolving novel concepts in imaging. The underlying principle is to use a large dataset of paired images (noisy input–high-quality output) in supervised training of an algorithm (also called neuronal networks) to recognize pattern and to extract features for classification. Importantly by correlating features (e.g., two correlating events in a cell) and applying a hierarchy, the algorithm 'learns' to extrapolate and predict cell (or subcellular) organizations, which allows cell identification, classification, and accurate image reconstitution in large populations. Input images can be derived from different sources including transmission light, fluorescence and live-cell microscopy and EM images, or combinations thereof [26,317–319]. Training such a network accurately identified rare events in which Ad-infected cells engage in lytic virus release. To train the algorithm, the authors stained nuclei in high-content live-cell imaging and used additional marker to train the network in discriminating infected cells. The resulting pattern of nuclear stain over time provided sufficient features to predict with > 95% accuracy Ad cell lysis [320].

Conclusions and perspectives

Imaging techniques have tremendously contributed to our spatial and temporal understanding of the Ad infection cycle. FM has made it possible to directly visualize and differentiate kinetic aspects in relation to the spatial organization of the virus during all phases of the Ad cycle. Labeling strategies for almost all viral and cellular components are applicable in a modular way to study the infection system, therefore allowing us to pinpoint specific events at a single-cell resolution and complementing biochemical and other assays that suffer from bulk measurement. FM of Ads has identified specific epitopes that can be used as optical detection marks to detect deterministic steps during the viral infection cycle such as endosomal escape (protein VI detection), capsid disassembly (exposure of hexon epitope), trafficking (MTOC accumulation), nuclear genome delivery (detection of protein VII or metabolically labeled genomes), and replication (detection of DBP). These marks enable a better description of interaction between Ad and its host, mostly in the context of antiviral immunity such as linking membrane damage to autophagy and genome sensing or the suppression of the DDR upon nuclear entry and during replication. Some imaging tools are still missing from the Ad imaging repertoire. Assembly and egress is one example awaiting the development of better labeling strategies and imaging tools to decipher the processes involved. Imaging of viral RNAs and gene expression is another example where existing tools have only provided limited information.

Developing FM for live-cell imaging of Ad-infected cells using labeling of viral and cellular structures allows tracking of viral capsids upon entry and genome delivery. This made it possible to extract kinetic information and generate tracking models and algorithms to describe the dynamic behavior of Ads in cells. It permits the detection and dissection of fast and transient events such as endocytosis and endosomal membrane penetration in real time, which was not possible in fixed cells or bulk analysis. The recent

development of labeling strategies for replication compartments and replicating, as well as incoming, viral genomes in living cells allowed the first complete dynamic description of the viral replication cycle. Novel labeling strategies for capsid assembly and egress should close the gap with the last step of the infection cycle. This may lead to experimental systems in which every step of the viral infection cycle is accessible to live-cell imaging, potentially identifying novel concepts or providing a spatiotemporal context to old observations, which will serve as future framework.

One aspect that has to be taken into consideration is that most FM imaging of Ads was done with AdC2/5 in easy-to-use cell culture models. In reality, both cell system and Ad genotype are important determinants for what can and will be observed. One example, described in this review, highlights how the viral genotype defines from which endosome the capsid escapes with consequences for immune activation. Thus, one should consider transferring the existing repertoire of FM imaging techniques presented in this review to alternative Ad species and more specialized and sophisticated cell models. In parallel, the development of new imaging techniques providing faster and higher resolution with the prospect to generate structural and mechanistic information gives us opportunities that make Ad imaging as exciting for future generations as it has been in the past.

The authors would like to apologize to colleagues whose work has not been mentioned in this review. The overwhelming amount of FM data for adenoviruses made it necessary to select limited examples to show principles for the application of FM in Ad imaging.

Acknowledgements

We would like to acknowledge support from the Fondation pour la Recherche Médicale (Equipes FRM 2018 DEQ20180339229). We thank the members of our group for their support and S.C. for help with the manuscript. Some of the microscopy was done in the Bordeaux Imaging Center, a service unit of the CNRS-INSERM, and Bordeaux University, a member of the national infrastructure France BioImaging. HW is an INSERM fellow.

References

1 Flint SJ and Nemerow GR (2016) Human Adenoviruses: From Villains to Vectors. World Scientific Publishing Co. Pte. Ltd., Singapore.
2 Rancourt C, Tihanyi K, Bourbonniere M and Weber JM (1994) Identification of active-site residues of the adenovirus endopeptidase. *Proc Natl Acad Sci USA* **91**, 844–847.
3 Imelli N, Ruzsics Z, Puntener D, Gastaldelli M and Greber UF (2009) Genetic reconstitution of the human adenovirus type 2 temperature-sensitive 1 mutant defective in endosomal escape. *Virol J* **6**, 174.
4 Dales S (1962) An electron microscope study of the early association between two mammalian viruses and their hosts. *J Cell Biol* **13**, 303–322.
5 Yoshimura A (1985) Adenovirus-induced leakage of co-endocytosed macromolecules into the cytosol. *Cell Struct Funct* **10**, 391–404.
6 Greber UF, Willetts M, Webster P and Helenius A (1993) Stepwise dismantling of adenovirus 2 during entry into cells. *Cell* **75**, 477–486.
7 Greber UF, Suomalainen M, Stidwill RP, Boucke K, Ebersold MW and Helenius A (1997) The role of the nuclear pore complex in adenovirus DNA entry. *EMBO J* **16**, 5998–6007.
8 Martin-Fernandez M, Longshaw SV, Kirby I, Santis G, Tobin MJ, Clarke DT and Jones GR (2004) Adenovirus type-5 entry and disassembly followed in living cells by FRET, fluorescence anisotropy, and FLIM. *Biophys J* **87**, 1316–1327.
9 Nevins JR, Ginsberg HS, Blanchard JM, Wilson MC and Darnell JE (1979) Regulation of the primary expression of the early adenovirus transcription units. *J Virol* **32**, 727–733.
10 Prusinkiewicz MA and Mymryk JS (2019) Metabolic reprogramming of the host cell by human adenovirus infection. *Viruses* **11**, 141.
11 Berk AJ (1986) Adenovirus promoters and E1A transactivation. *Annu Rev Genet* **20**, 45–79.
12 Weitzman MD and Ornelles DA (2005) Inactivating intracellular antiviral responses during adenovirus infection. *Oncogene* **24**, 7686–7696.
13 Flint SJ and Gonzalez RA (2003) Regulation of mRNA production by the adenoviral E1B 55-kDa and E4 Orf6 proteins. *Curr Top Microbiol Immunol* **272**, 287–330.
14 San Martín C (2012) Latest insights on adenovirus structure and assembly. *Viruses* **4**, 847–877.
15 Mangel WF and San Martín C (2014) Structure, function and dynamics in adenovirus maturation. *Viruses* **6**, 4536–4570.
16 Kjellén L, Lagermalm G, Svedmyr A and Thorsson K-G (1955) Crystalline-like patterns in the nuclei of cells infected with an animal virus. *Nature* **175**, 505–506.
17 Harford CG (1956) Electron microscopy of HeLa cells infected with adenoviruses. *J Exp Med* **104**, 443–454.
18 Rowe WP, Huebner RJ, Gilmore LK, Parrott RH and Ward TG (1953) Isolation of a cytopathogenic agent from human adenoids undergoing spontaneous degeneration in tissue culture. *Proc Soc Exp Biol Med* **84**, 570–573.

19 Boyer GS, Leuchtenberger C and Ginsberg HS (1957) Cytological and cytochemical studies of Hela cells infected with adenoviruses. *J. Exp. Med.* **105**, 195–216.
20 Pereira HG, Allison AC and Balfour B (1959) Multiplication of adenovirus type 5 studied by infectivity titrations and by the fluorescent antibody technique. *Virology* **7**, 300–314.
21 Gilead Z and Ginsberg HS (1965) Characterization of a tumorlike antigen in type 12 and type 18 adenovirus-infected cells. *J Bacteriol* **90**, 120–125.
22 Hayashi K and Russell WC (1968) A study of the development of adenovirus antigens by the immunofluorescent technique. *Virology* **34**, 470–480.
23 Persson R, Svensson U and Everitt E (1983) Virus receptor interaction in the adenovirus system. *J Virol* **46**, 8.
24 Svensson U and Persson R (1984) Entry of adenovirus 2 into HeLa cells. *J Virol* **51**, 8.
25 Witte R, Andriasyan V, Georgi F, Yakimovich A and Greber UF (2018) Concepts in light microscopy of viruses. *Viruses* **10**, 202.
26 Wang I-H, Burckhardt C, Yakimovich A and Greber U (2018) Imaging, tracking and computational analyses of virus entry and egress with the cytoskeleton. *Viruses* **10**, 166.
27 Müller TG, Sakin V and Müller B (2019) A spotlight on viruses—application of click chemistry to visualize virus-cell interactions. *Molecules* **24**, 481.
28 Wisnivesky JP, Leopold PL and Crystal RG (1999) Specific binding of the adenovirus capsid to the nuclear envelope. *Hum Gene Ther* **10**, 2187–2195.
29 Glotzer JB, Michou AI, Baker A, Saltik M and Cotten M (2001) Microtubule-independent motility and nuclear targeting of adenoviruses with fluorescently labeled genomes. *J Virol* **75**, 2421–2434.
30 Bailey CJ, Crystal RG and Leopold PL (2003) Association of adenovirus with the microtubule organizing center. *J Virol* **77**, 13275–13287.
31 Bremner KH, Scherer J, Yi J, Vershinin M, Gross SP and Vallee RB (2009) Adenovirus transport through a direct cytoplasmic dynein-hexon interaction. *Cell Host Microbe* **6**, 523–535.
32 Zhou J, Scherer J, Yi J and Vallee RB (2018) Role of kinesins in directed adenovirus transport and cytoplasmic exploration. *PLoS Pathog* **14**, e1007055.
33 Burckhardt CJ, Suomalainen M, Schoenenberger P, Boucke K, Hemmi S and Greber UF (2011) Drifting motions of the adenovirus receptor CAR and immobile integrins initiate virus uncoating and membrane lytic protein exposure. *Cell Host Microbe* **10**, 105–117.
34 Ortega-Esteban A, Bodensiek K, San Martín C, Suomalainen M, Greber UF, de Pablo PJ and Schaap IAT (2015) Fluorescence tracking of genome release during mechanical unpacking of single viruses. *ACS Nano* **9**, 10571–10579.
35 Minsky M (1988) Memoir on inventing the confocal scanning microscope. *Scanning* **10**, 128–138.
36 Suomalainen M, Luisoni S, Boucke K, Bianchi S, Engel DA and Greber UF (2013) A direct and versatile assay measuring membrane penetration of adenovirus in single cells. *J Virol* **87**, 12367–12379.
37 Nakano MY, Boucke K, Suomalainen M, Stidwill RP and Greber UF (2000) The first step of adenovirus type 2 disassembly occurs at the cell surface, independently of endocytosis and escape to the cytosol. *J Virol* **74**, 7085–7095.
38 Varghese R, Mikyas Y, Stewart PL and Ralston R (2004) Postentry neutralization of adenovirus type 5 by an antihexon antibody. *J Virol* **78**, 12320–12332.
39 Warren JC, Rutkowski A and Cassimeris L (2006) Infection with replication-deficient adenovirus induces changes in the dynamic instability of host cell microtubules. *Mol Biol Cell* **17**, 3557–3568.
40 Wodrich H, Henaff D, Jammart B, Segura-Morales C, Seelmeir S, Coux O, Ruzsics Z, Wiethoff CM and Kremer EJ (2010) A capsid-encoded PPxY-motif facilitates adenovirus entry. *PLoS Pathog* **6**, e1000808.
41 Engelke MF, Burckhardt CJ, Morf MK and Greber UF (2011) The dynactin complex enhances the speed of microtubule-dependent motions of adenovirus both towards and away from the nucleus. *Viruses* **3**, 233–253.
42 Komatsu T, Dacheux D, Kreppel F, Nagata K and Wodrich H (2015) A method for visualization of incoming adenovirus chromatin complexes in fixed and living cells. *PLoS ONE* **10**, e0137102.
43 Wang I-H, Burckhardt CJ, Yakimovich A, Morf MK and Greber UF (2017) The nuclear export factor CRM1 controls juxta-nuclear microtubule-dependent virus transport. *J Cell Sci* **130**, 2185–2195.
44 Jonkman J and Brown CM (2015) Any way you slice it-a comparison of confocal microscopy techniques. *J Biomol Tech* **26**, 54–65.
45 Avgousti DC, Herrmann C, Kulej K, Pancholi NJ, Sekulic N, Petrescu J, Molden RC, Blumenthal D, Paris AJ, Reyes ED *et al.* (2016) A core viral protein binds host nucleosomes to sequester immune danger signals. *Nature* **535**, 173–177.
46 Komatsu T, Quentin-Froignant C, Carlon-Andres I, Lagadec F, Rayne F, Ragues J, Kehlenbach RH, Zhang W, Ehrhardt A, Bystricky K *et al.* (2018) *In vivo* labelling of adenovirus DNA identifies chromatin anchoring and biphasic genome replication. *J Virol* **92**, e00795-18.
47 Abbe E (1873) Beiträge zur Theorie des Mikroskops und der mikroskopischen Wahrnehmung. *Arch Mikrosk Anat* **9**, 413–468.
48 Wegel E, Göhler A, Lagerholm BC, Wainman A, Uphoff S, Kaufmann R and Dobbie IM (2016) Imaging cellular structures in super-resolution with

SIM, STED and localisation microscopy: a practical comparison. *Sci Rep* **6**, 27290.
49 Wang I-H, Suomalainen M, Andriasyan V, Kilcher S, Mercer J, Neef A, Luedtke NW and Greber UF (2013) Tracking viral genomes in host cells at single-molecule resolution. *Cell Host Microbe* **14**, 468–480.
50 Henriques R, Griffiths C, Hesper Rego E and Mhlanga MM (2011) PALM and STORM: unlocking live-cell super-resolution. *Biopolymers* **95**, 322–331.
51 Shashkova S and Leake MC (2017) Single-molecule fluorescence microscopy review: shedding new light on old problems. *Biosci Rep* **37**, BSR20170031.
52 Russell WC and Knight BE (1967) Evidence for a new antigen within the adenovirus capsid. *J Gen Virol* **1**, 523–528.
53 Levinson A, Levine AJ, Anderson S, Osborn M, Rosenwirth B and Weber K (1976) The relationship between group C adenovirus tumor antigen and the adenovirus single-strand DNA-binding protein. *Cell* **7**, 575–584.
54 Sugawara K, Gilead Z, Wold WS and Green M (1977) Immunofluorescence study of the adenovirus type 2 single-stranded DNA binding protein in infected and transformed cells. *J Virol* **13**, 527–539.
55 Levinson A and Levine AJ (1977) The isolation and identification of the adenovirus group C tumor antigens. *Virology* **76**, 1–11.
56 Lassam NJ, Bayley ST and Graham FL (1979) Tumor antigens of human Ad5 in transformed cells and in cells infected with transformation-defective host-range mutants. *Cell* **18**, 781–791.
57 Sarnow P, Sullivan CA and Levine AJ (1982) A monoclonal antibody detecting the adenovirus type 5–E1b-58Kd tumor antigen: characterization of the E1b–58Kd tumor antigen in adenovirus-infected and -transformed cells. *Virology* **120**, 510–517.
58 Greber UF, Nakano MY and Suomalainen M (1998) Adenovirus entry into cells: a quantitative fluorescence microscopy approach. In Adenovirus Methods and Protocols (Wold WSM, ed), Vol. **21**, pp. 217–230. Humana Press, Wayne, NJ.
59 Leopold PL, Ferris B, Grinberg I, Worgall S, Hackett NR and Crystal RG (1998) Fluorescent virions: dynamic tracking of the pathway of adenoviral gene transfer vectors in living cells. *Hum Gene Ther* **9**, 367–378.
60 Leopold PL, Kreitzer G, Miyazawa N, Rempel S, Pfister KK, Rodriguez-Boulan E and Crystal RG (2000) Dynein- and microtubule-mediated translocation of adenovirus serotype 5 occurs after endosomal lysis. *Hum Gene Ther* **11**, 151–165.
61 Soudais C, Boutin S, Hong SS, Chillon M, Danos O, Bergelson JM, Boulanger P and Kremer EJ (2000) Canine adenovirus type 2 attachment and internalization: coxsackievirus-adenovirus receptor, alternative receptors, and an RGD-independent pathway. *J Virol* **74**, 10639–10649.
62 Wodrich H, Guan T, Cingolani G, Von Seggern D, Nemerow G and Gerace L (2003) Switch from capsid protein import to adenovirus assembly by cleavage of nuclear transport signals. *EMBO J* **22**, 6245–6255.
63 Herod MR, Pineda RG, Mautner V and Onion D (2015) Quantum dot labelling of adenovirus allows highly sensitive single cell flow and imaging cytometry. *Small Weinh Bergstr Ger* **11**, 797–803.
64 Martinez R, Burrage AM, Wiethoff CM and Wodrich H (2013) High temporal resolution imaging reveals endosomal membrane penetration and escape of adenoviruses in real time. *Methods Mol Biol* **1064**, 211–226.
65 Espenlaub S, Corjon S, Engler T, Fella C, Ogris M, Wagner E, Kochanek S and Kreppel F (2010) Capsomer-specific fluorescent labeling of adenoviral vector particles allows for detailed analysis of intracellular particle trafficking and the performance of bioresponsive bonds for vector capsid modifications. *Hum Gene Ther* **21**, 1155–1167.
66 Banerjee PS, Ostapchuk P, Hearing P and Carrico IS (2011) Unnatural amino acid incorporation onto adenoviral (Ad) coat proteins facilitates chemoselective modification and retargeting of Ad type 5 vectors. *J Virol* **85**, 7546–7554.
67 Rubino FA, Oum YH, Rajaram L, Chu Y and Carrico IS (2012) Chemoselective modification of viral surfaces via bioorthogonal click chemistry. *J Vis Exp* **66**, e4246.
68 Banerjee PS, Ostapchuk P, Hearing P and Carrico I (2010) Chemoselective attachment of small molecule effector functionality to human adenoviruses facilitates gene delivery to cancer cells. *J Am Chem Soc* **132**, 13615–13617.
69 Ouyang T, Liu X, Ouyang H and Ren L (2018) Recent trends in click chemistry as a promising technology for virus-related research. *Virus Res* **256**, 21–28.
70 Tsien RY (1998) The green fluorescent protein. *Annu Rev Biochem* **67**, 509–544.
71 Le LP, Everts M, Dmitriev IP, Davydova JG, Yamamoto M and Curiel DT (2004) Fluorescently labeled adenovirus with pIX-EGFP for vector detection. *Mol Imaging* **3**, 105–116.
72 Meulenbroek RA, Sargent KL, Lunde J, Jasmin BJ and Parks RJ (2004) Use of adenovirus protein IX (pIX) to display large polypeptides on the virion–generation of fluorescent virus through the incorporation of pIX-GFP. *Mol Ther* **9**, 617–624.
73 Le LP, Le HN, Nelson AR, Matthews DA, Yamamoto M and Curiel DT (2006) Core labeling of adenovirus with EGFP. *Virology* **351**, 291–302.
74 Kimball KJ, Rivera AA, Zinn KR, Icyuz M, Saini V, Li J, Zhu ZB, Siegal GP, Douglas JT, Curiel DT *et al*.

(2009) Novel infectivity-enhanced oncolytic adenovirus with a capsid-incorporated dual-imaging moiety for monitoring virotherapy in ovarian cancer. *Mol Imaging* **8**, 264–277.
75 Ugai H, Wang M, Le LP, Matthews DA, Yamamoto M and Curiel DT (2010) In vitro dynamic visualization analysis of fluorescently labeled minor capsid protein IX and core protein V by simultaneous detection. *J Mol Biol* **395**, 55–78.
76 Puntener D, Engelke MF, Ruzsics Z, Strunze S, Wilhelm C and Greber UF (2011) Stepwise loss of fluorescent core protein V from human adenovirus during entry into cells. *J Virol* **85**, 481–496.
77 Yang M, Baranov E, Moossa AR, Penman S and Hoffman RM (2000) Visualizing gene expression by whole-body fluorescence imaging. *Proc Natl Acad Sci USA* **97**, 12278–12282.
78 Lee C-T, Lee Y-J, Kwon S-Y, Lee J, Kim KI, Park K-H, Kang JH, Yoo C-G, Kim YW, Han SK *et al*. (2006) In vivo imaging of adenovirus transduction and enhanced therapeutic efficacy of combination therapy with conditionally replicating adenovirus and adenovirus-p27. *Cancer Res* **66**, 372–377.
79 Guse K, Dias JD, Bauerschmitz GJ, Hakkarainen T, Aavik E, Ranki T, Pisto T, Särkioja M, Desmond RA, Kanerva A *et al*. (2007) Luciferase imaging for evaluation of oncolytic adenovirus replication in vivo. *Gene Ther* **14**, 902–911.
80 Borovjagin AV, McNally LR, Wang M, Curiel DT, MacDougall MJ and Zinn KR (2010) Noninvasive monitoring of mRFP1- and mCherry-labeled oncolytic adenoviruses in an orthotopic breast cancer model by spectral imaging. *Mol Imaging* **9**, 59–75.
81 Barry MA, May S and Weaver EA (2012) Imaging luciferase-expressing viruses. *Methods Mol Biol* **797**, 79–87.
82 Mehle A (2015) Fiat Luc: bioluminescence imaging reveals in vivo viral replication dynamics. *PLoS Pathog* **11**, e1005081.
83 Coleman SM and McGregor A (2015) A bright future for bioluminescent imaging in viral research. *Future Virol* **10**, 169–183.
84 Sewald X (2018) Visualizing viral infection in vivo by multi-photon intravital microscopy. *Viruses* **10**, 337.
85 Bauman JG, Wiegant J, Borst P and van Duijn P (1980) A new method for fluorescence microscopical localization of specific DNA sequences by in situ hybridization of fluorochrome-labelled RNA. *Exp Cell Res* **128**, 485–490.
86 Bauman JG and van Duijn P (1981) Hybrido-cytochemical localization of specific DNA sequences by fluorescence microscopy. *Histochem J* **13**, 723–733.
87 Brigati DJ, Myerson D, Leary JJ, Spalholz B, Travis SZ, Fong CKY, Hsiung GD and Ward DC (1983) Detection of viral genomes in cultured cells and paraffin-embedded tissue sections using biotin-labeled hybridization probes. *Virology* **126**, 32–50.
88 Pombo A, Ferreira J, Bridge E and Carmo-Fonseca M (1994) Adenovirus replication and transcription sites are spatially separated in the nucleus of infected cells. *EMBO J* **13**, 5075–5085.
89 Komatsu T, Robinson DR, Hisaoka M, Ueshima S, Okuwaki M, Nagata K and Wodrich H (2016) Tracking adenovirus genomes identifies morphologically distinct late DNA replication compartments. *Traffic* **17**, 1168–1180.
90 Nguyen EK, Nemerow GR and Smith JG (2010) Direct evidence from single-cell analysis that human α-defensins block adenovirus uncoating to neutralize infection. *J Virol* **84**, 4041–4049.
91 Condezo GN and San Martín C (2017) Localization of adenovirus morphogenesis players, together with visualization of assembly intermediates and failed products, favor a model where assembly and packaging occur concurrently at the periphery of the replication center. *PLOS Pathog* **13**, e1006320.
92 Xue Y, Johnson JS, Ornelles DA, Lieberman J and Engel DA (2005) adenovirus protein VII functions throughout early phase and interacts with cellular proteins SET and pp32. *J Virol* **79**, 2474–2483.
93 Chen J, Morral N and Engel DA (2007) Transcription releases protein VII from adenovirus chromatin. *Virology* **369**, 411–422.
94 Komatsu T and Nagata K (2012) Replication-uncoupled histone deposition during adenovirus DNA replication. *J Virol* **86**, 6701–6711.
95 Saad H, Gallardo F, Dalvai M, Tanguy-le-Gac N, Lane D and Bystricky K (2014) DNA dynamics during early double-strand break processing revealed by non-intrusive imaging of living cells. *PLOS Genet* **10**, e1004187.
96 Kilgore JA, Dolman NJ and Davidson MW (2013) A review of reagents for fluorescence microscopy of cellular compartments and structures, Part II: reagents for non-vesicular organelles. *Curr Protoc Cytom* **66**, Unit 12.31.
97 Minamikawa T, Sriratana A, Williams DA, Bowser DN, Hill JS and Nagley P (1999) Chloromethyl-X-rosamine (MitoTracker Red) photosensitises mitochondria and induces apoptosis in intact human cells. *J Cell Sci* **112** (Pt 14), 2419–2430.
98 Dingsdale H, Haynes LP, Tepikin AV and Lur G (2011) Visualising the endoplasmic reticulum and its contacts with other organelles in live acinar cells. American Pancreatic Association APA, University of Michigan, Ann Arbor.
99 Chazotte B (2011) Labeling lysosomes in live cells with LysoTracker. *Cold Spring Harb Protoc* **2011**, pdb.prot5571.
100 Pryor PR (2012) Chapter eight – analyzing lysosomes in live cells. In Methods in Enzymology (Conn PM, ed.), pp. 145–157. Academic Press, Cambridge, MA.

101 Lukinavičius G, Reymond L, D'Este E, Masharina A, Göttfert F, Ta H, Güther A, Fournier M, Rizzo S, Waldmann H *et al*. (2014) Fluorogenic probes for live-cell imaging of the cytoskeleton. *Nat Methods* **11**, 731–733.
102 Khodabakhsh F, Behdani M, Rami A and Kazemi-Lomedasht F (2018) Single-domain antibodies or nanobodies: a class of next-generation antibodies. *Int Rev Immunol* **37**, 316–322.
103 Traenkle B and Rothbauer U (2017) Under the microscope: single-domain antibodies for live-cell imaging and super-resolution microscopy. *Front Immunol* **8**, 1030.
104 Rothbauer U, Zolghadr K, Tillib S, Nowak D, Schermelleh L, Gahl A, Backmann N, Conrath K, Muyldermans S, Cardoso MC *et al*. (2006) Targeting and tracing antigens in live cells with fluorescent nanobodies. *Nat Methods* **3**, 887–889.
105 Ries J, Kaplan C, Platonova E, Eghlidi H and Ewers H (2012) A simple, versatile method for GFP-based super-resolution microscopy via nanobodies. *Nat Methods* **9**, 582–584.
106 Keller B-M, Maier J, Secker K-A, Egetemaier S-M, Parfyonova Y, Rothbauer U and Traenkle B (2018) Chromobodies to quantify changes of endogenous protein concentration in living cells. *Mol Cell Proteomics* **17**, 2518–2533.
107 Groneberg J, Brown DT and Doerfler W (1975) Uptake and fate of the DNA of adenovirus type 2 in KB cells. *Virology* **64**, 115–131.
108 Laughlin CA, Cardellichio CB and Coon HC (1986) Latent infection of KB cells with adeno-associated virus type 2. *J Virol* **60**, 515–524.
109 Carey B, Staudt MK, Bonaminio D, van der Loo JCM and Trapnell BC (2007) PU.1 redirects adenovirus to lysosomes in alveolar macrophages, uncoupling internalization from infection. *J Immunol* **178**, 2440–2447.
110 Maier O, Marvin SA, Wodrich H, Campbell EM and Wiethoff CM (2012) Spatiotemporal dynamics of adenovirus membrane rupture and endosomal escape. *J Virol* **86**, 10821–10828.
111 Montespan C, Marvin SA, Austin S, Burrage AM, Roger B, Rayne F, Faure M, Campell EM, Schneider C, Reimer R *et al*. (2017) Multi-layered control of Galectin-8 mediated autophagy during adenovirus cell entry through a conserved PPxY motif in the viral capsid. *PLOS Pathog* **13**, e1006217.
112 Zhang Y and Bergelson JM (2005) Adenovirus receptors. *J Virol* **79**, 12125–12131.
113 Arnberg N (2012) Adenovirus receptors: implications for targeting of viral vectors. *Trends Pharmacol Sci* **33**, 442–448.
114 Defer C, Belin M-T, Caillet-Boudin M-L and Boulanger P (1990) Human adenovirus-host cell interactions: comparative study with members of subgroups B and C. *J Virol* **64**, 13.
115 Ebbinghaus C, Al-Jaibaji A, Operschall E, Schöffel A, Peter I, Greber UF and Hemmi S (2001) Functional and selective targeting of adenovirus to high-affinity Fcγ receptor I-positive cells by using a bispecific hybrid adapter. *J Virol* **75**, 480–489.
116 Kaner RJ, Worgall S, Leopold PL, Stolze E, Milano E, Hidaka C, Ramalingam R, Hackett NR, Singh R, Bergelson J *et al*. (1999) Modification of the genetic program of human alveolar macrophages by adenovirus vectors in vitro is feasible but inefficient, limited in part by the low level of expression of the coxsackie/adenovirus receptor. *Am J Respir Cell Mol Biol* **20**, 361–370.
117 Salinas S, Zussy C, Loustalot F, Henaff D, Menendez G, Morton PE, Parsons M, Schiavo G and Kremer EJ (2014) Disruption of the coxsackievirus and adenovirus receptor-homodimeric interaction triggers lipid microdomain- and dynamin-dependent endocytosis and lysosomal targeting. *J Biol Chem* **289**, 680–695.
118 Leopold PL and Crystal RG (2007) Intracellular trafficking of adenovirus: Many means to many ends. *Adv Drug Deliv Rev* **59**, 810–821.
119 Hidaka C, Milano E, Leopold PL, Bergelson JM, Hackett NR, Finberg RW, Wickham TJ, Kovesdi I, Roelvink P and Crystal RG (1999) CAR-dependent and CAR-independent pathways of adenovirus vector-mediated gene transfer and expression in human fibroblasts. *J Clin Invest* **103**, 579–587.
120 Bailey CJCR and Leopold PL (2003) Unlike most cell types, translocation of the adenovirus genome to the nucleus of endothelial cells is not associated with nuclear localization of the adenovirus capsid. *Mol Ther* **7**, S55.
121 Zaiss AK, Vilaysane A, Cotter MJ, Clark SA, Meijndert HC, Colarusso P, Yates RM, Petrilli V, Tschopp J and Muruve DA (2009) Antiviral antibodies target adenovirus to phagolysosomes and amplify the innate immune response. *J Immunol* **182**, 7058–7068.
122 Eichholz K, Bru T, Tran TTP, Fernandes P, Welles H, Mennechet FJD, Manel N, Alves P, Perreau M and Kremer EJ (2016) Immune-complexed adenovirus induce AIM2-mediated pyroptosis in human dendritic cells. *PLOS Pathog* **12**, e1005871.
123 Tippimanchai DD, Nolan K, Poczobutt J, Verzosa G, Li H, Scarborough H, Huang J, Young C, DeGregori J, Nemenoff RA *et al*. (2018) Adenoviral vectors transduce alveolar macrophages in lung cancer models. *Oncoimmunology* **7**, e1438105.
124 Patterson S and Russell WC (1983) Ultrastructural and immunofluorescence studies of early events in adenovirus-HeLa cell interactions. *J Gen Virol* **64**, 1091–1099.

125 Belin M-T and Boulanger P (1993) Involvement of cellular adhesion sequences in the attachment of adenovirus to the HeLa cell surface. *J Gen Virol* **74**, 1485–1497.
126 Wickham TJ, Mathias P, Cheresh DA and Nemerow GR (1993) Integrins αvβ3 and αvβ5 promote adenovirus internalization but not virus attachment. *Cell* **73**, 309–319.
127 Bergelson JM, Cunningham JA, Droguett G, Kurt-Jones EA, Krithivas A, Hong JS, Horwitz MS, Crowell RL and Finberg RW (1997) Isolation of a common receptor for Coxsackie B viruses and adenoviruses 2 and 5. *Science* **275**, 1320–1323.
128 Helmuth JA, Burckhardt CJ, Koumoutsakos P, Greber UF and Sbalzarini IF (2007) A novel supervised trajectory segmentation algorithm identifies distinct types of human adenovirus motion in host cells. *J Struct Biol* **159**, 347–358.
129 Morgan C, Howe C and Rose HM (1961) Structure and development of viruses as observed in the electron microscope. *J. Exp. Med.* **113**, 219–234.
130 Brown DT and Burlingham BT (1973) Penetration of host cell membranes by adenovirus 2. *J Virol* **12**, 11.
131 Meier O, Boucke K, Hammer SV, Keller S, Stidwill RP, Hemmi S and Greber UF (2002) Adenovirus triggers macropinocytosis and endosomal leakage together with its clathrin-mediated uptake. *J Cell Biol* **158**, 1119–1131.
132 Gastaldelli M, Imelli N, Boucke K, Amstutz B, Meier O and Greber UF (2008) Infectious adenovirus type 2 transport through early but not late endosomes. *Traffic* **9**, 2265–2278.
133 Greber UF, Webster P, Weber J and Helenius A (1996) The role of the adenovirus protease on virus entry into cells. *EMBO J* **15**, 1766–1777.
134 Arnberg N, Edlund K, Kidd AH and Wadell G (2000) Adenovirus type 37 uses sialic acid as a cellular receptor. *J Virol* **74**, 42–48.
135 Miyazawa N, Leopold PL, Hackett NR, Ferris B, Worgall S, Falck-Pedersen E and Crystal RG (1999) Fiber swap between adenovirus subgroups B and C alters intracellular trafficking of adenovirus gene transfer vectors. *J Virol* **73**, 6056–6065.
136 Miyazawa N, Crystal RG and Leopold PL (2001) Adenovirus serotype 7 retention in a late endosomal compartment prior to cytosol escape is modulated by fiber protein. *J Virol* **75**, 1387–1400.
137 Yousuf MA, Zhou X, Mukherjee S, Chintakuntlawar AV, Lee JY, Ramke M, Chodosh J and Rajaiya J (2013) Caveolin-1 associated adenovirus entry into human corneal cells. *PLoS ONE* **8**, e77462.
138 Fernández-Puentes C and Carrasco L (1980) Viral infection permeabilizes mammalian cells to protein toxins. *Cell* **20**, 769–775.
139 FitzGerald DJ, Padmanabhan R, Pastan I and Willingham MC (1983) Adenovirus-induced release of epidermal growth factor and pseudomonas toxin into the cytosol of KB cells during receptor-mediated endocytosis. *Cell* **32**, 607–617.
140 Wickham TJ (1994) Integrin alpha v beta 5 selectively promotes adenovirus mediated cell membrane permeabilization. *J Cell Biol* **127**, 257–264.
141 Wang K, Guan T, Cheresh DA and Nemerow GR (2000) Regulation of adenovirus membrane penetration by the cytoplasmic tail of integrin β5. *J Virol* **74**, 9.
142 Wiethoff CM, Wodrich H, Gerace L and Nemerow GR (2005) Adenovirus protein VI mediates membrane disruption following capsid disassembly. *J Virol* **79**, 1992–2000.
143 Maier O and Wiethoff CM (2010) N-terminal α-helix-independent membrane interactions facilitate adenovirus protein VI induction of membrane tubule formation. *Virology* **408**, 31–38.
144 Luisoni S, Suomalainen M, Boucke K, Tanner LB, Wenk MR, Guan XL, Grzybek M, Coskun Ü and Greber UF (2015) Co-option of membrane wounding enables virus penetration into cells. *Cell Host Microbe* **18**, 75–85.
145 Paz I, Sachse M, Dupont N, Mounier J, Cederfur C, Enninga J, Leffler H, Poirier F, Prevost M-C, Lafont F *et al.* (2010) Galectin-3, a marker for vacuole lysis by invasive pathogens. *Cell Microbiol* **12**, 530–544.
146 Martinez R, Schellenberger P, Vasishtan D, Aknin C, Austin S, Dacheux D, Rayne F, Siebert A, Ruzsics Z, Gruenewald K *et al.* (2015) The amphipathic helix of adenovirus capsid protein VI contributes to penton release and postentry sorting. *J Virol* **89**, 2121–2135.
147 Luisoni S, Bauer M, Prasad V, Boucke K, Papadopoulos C, Meyer H, Hemmi S, Suomalainen M and Greber UF (2016) Endosomophagy clears disrupted early endosomes but not virus particles during virus entry into cells. *Matters* **2**, e201606000013.
148 Moyer CL, Wiethoff CM, Maier O, Smith JG and Nemerow GR (2011) Functional genetic and biophysical analyses of membrane disruption by human adenovirus. *J Virol* **85**, 2631–2641.
149 Deretic V and Levine B (2018) Autophagy balances inflammation in innate immunity. *Autophagy* **14**, 243–251.
150 Naghavi MH and Walsh D (2017) Microtubule regulation and function during virus infection. *J Virol* **91**, e00538-17.
151 Dales S and Chardonnet Y (1970) Early events in the interaction of adenoviruses with HeLa cells. I. Penetration of type 5 and intracellular release of the DNA genome. *Virology* **40**, 462–477.
152 Miles BD, Luftig RB, Weatherbee JA, Weihing RR and Weber J (1980) Quantitation of the interaction between adenovirus types 2 and 5 and microtubules inside infected cells. *Virology* **105**, 265–269.

153 Suomalainen M, Nakano MY, Keller S, Boucke K, Stidwill RP and Greber UF (1999) Microtubule-dependent plus- and minus end-directed motilities are competing processes for nuclear targeting of adenovirus. *J Cell Biol* **144**, 657–672.
154 Kelkar SA, Pfister KK, Crystal RG and Leopold PL (2004) Cytoplasmic dynein mediates adenovirus binding to microtubules. *J Virol* **78**, 10122–10132.
155 Luftig RB and Weihing RR (1975) Adenovirus binds to rat brain microtubules in vitro. *J Virol* **16**, 696–706.
156 Smith JG, Cassany A, Gerace L, Ralston R and Nemerow GR (2008) Neutralizing antibody blocks adenovirus infection by arresting microtubule-dependent cytoplasmic transport. *J Virol* **82**, 6492–6500.
157 Bremner KH, Scherer J, Yi J, Vershinin M, Gross SP and Vallee RB (2009) Adenovirus transport via direct interaction of cytoplasmic dynein with the viral capsid hexon subunit. *Cell Host Microbe* **6**, 523–535.
158 Leopold P and Crystal R (2007) Intracellular trafficking of adenovirus: many means to many ends. *Adv Drug Deliv Rev* **59**, 810–821.
159 Strunze S, Trotman LC, Boucke K and Greber UF (2005) Nuclear targeting of adenovirus type 2 requires CRM1-mediated nuclear export. *Mol Biol Cell* **16**, 11.
160 Yea C, Dembowy J, Pacione L and Brown M (2007) Microtubule-mediated and microtubule-independent transport of adenovirus type 5 in HEK293 cells. *J Virol* **81**, 6899–6908.
161 Chardonnet Y and Dales S (1972) Early events in the interaction of adenoviruses with HeLa cells. 3. Relationship between an ATPase activity in nuclear envelopes and transfer of core material: a hypothesis. *Virology* **48**, 342–359.
162 Saphire AC, Guan T, Schirmer EC, Nemerow GR and Gerace L (2000) Nuclear import of adenovirus DNA in vitro involves the nuclear protein import pathway and hsc70. *J Biol Chem* **275**, 4298–4304.
163 Baum SG, Horwitz MS and Maizel JV (1972) Studies of the mechanism of enhancement of human adenovirus infection in monkey cells by Simian virus 40. *J Virol* **10**, 9.
164 Trotman LC, Mosberger N, Fornerod M, Stidwill RP and Greber UF (2001) Import of adenovirus DNA involves the nuclear pore complex receptor CAN/Nup214 and histone H1. *Nat Cell Biol* **3**, 1092–1100.
165 Strunze S, Engelke MF, Wang I-H, Puntener D, Boucke K, Schleich S, Way M, Schoenenberger P, Burckhardt CJ and Greber UF (2011) Kinesin-1-mediated capsid disassembly and disruption of the nuclear pore complex promote virus infection. *Cell Host Microbe* **10**, 210–223.
166 Cassany A, Ragues J, Guan T, Bégu D, Wodrich H, Kann M, Nemerow GR and Gerace L (2015) Nuclear import of adenovirus DNA involves direct interaction of hexon with an N-terminal domain of the nucleoporin Nup214. *J Virol* **89**, 1719–1730.
167 Panté N and Kann M (2002) Nuclear pore complex is able to transport macromolecules with diameters of ~39 nm. *Mol Biol Cell* **13**, 425–434.
168 Zur Hausen H (1968) Persistence of the viral genome in adenovirus type 12-infected hamster cells. *J Virol* **2**, 918–924.
169 Zur Hausen H (1968) Association of adenovirus type 12 deoxyribonucleic acid with host cell chromosomes. *J Virol* **2**, 218–223.
170 Bauman JG, Wiegant J and van Duijn P (1981) Cytochemical hybridization with fluorochrome-labeled RNA. II. Applications. *J Histochem Cytochem* **29**, 238–246.
171 Hama S, Akita H, Iida S, Mizuguchi H and Harashima H (2007) Quantitative and mechanism-based investigation of post-nuclear delivery events between adenovirus and lipoplex. *Nucleic Acids Res* **35**, 1533–1543.
172 Hindley CE, Lawrence FJ and Matthews DA (2007) A role for transportin in the nuclear import of adenovirus core proteins and DNA. *Traffic* **8**, 1313–1322.
173 Lee TWR (2003) Adenovirus core protein VII contains distinct sequences that mediate targeting to the nucleus and nucleolus, and colocalization with human chromosomes. *J Gen Virol* **84**, 3423–3428.
174 Wodrich H, Cassany A, D'Angelo MA, Guan T, Nemerow G and Gerace L (2006) Adenovirus core protein pVII is translocated into the nucleus by multiple import receptor pathways. *J Virol* **80**, 9608–9618.
175 Walkiewicz MP, Morral N and Engel DA (2009) Accurate single-day titration of adenovirus vectors based on equivalence of protein VII nuclear dots and infectious particles. *J Virol Methods* **159**, 251–258.
176 Haruki H, Gyurcsik B, Okuwaki M and Nagata K (2003) Ternary complex formation between DNA-adenovirus core protein VII and TAF-Iβ/SET, an acidic molecular chaperone. *FEBS Lett* **555**, 521–527.
177 Johnson JS, Osheim YN, Xue Y, Emanuel MR, Lewis PW, Bankovich A, Beyer AL and Engel DA (2004) Adenovirus protein VII condenses DNA, represses transcription, and associates with transcriptional activator E1A. *J Virol* **78**, 6459–6468.
178 Ross PJ, Kennedy MA, Christou C, Quiroz MR, Poulin KL and Parks RJ (2011) Assembly of helper-dependent adenovirus DNA into chromatin promotes efficient gene expression. *J Virol* **85**, 3950–3958.
179 Giberson AN, Davidson AR and Parks RJ (2012) Chromatin structure of adenovirus DNA throughout infection. *Nucleic Acids Res* **40**, 2369–2376.
180 Haruki H, Okuwaki M, Miyagishi M, Taira K and Nagata K (2006) Involvement of template-activating

factor I/SET in transcription of adenovirus early genes as a positive-acting factor. *J Virol* **80**, 794–801.
181 Fredman JN and Engler JA (1993) Adenovirus precursor to terminal protein interacts with the nuclear matrix in vivo and in vitro. *J Virol* **67**, 3384–3395.
182 Berk AJ, Lee F, Harrison T, Williams J and Sharp PA (1979) Pre-early adenovirus 5 gene product regulates synthesis of early viral messenger RNAs. *Cell* **17**, 935–944.
183 Thomas GP and Mathews MB (1980) DNA replication and the early to late transition in adenovirus infection. *Cell* **22**, 523–533.
184 Nevins JR (1981) Mechanism of activation of early viral transcription by the adenovirus E1A gene product. *Cell* **26**, 213–220.
185 Flint SJ (1986) Regulation of adenovirus mRNA formation. *Adv Virus Res* **31**, 169–228.
186 Nevins JR (1987) Regulation of early adenovirus gene expression. *Microbiol Rev* **51**, 419–430.
187 Farley DC, Brown JL and Leppard KN (2004) Activation of the early-late switch in adenovirus type 5 major late transcription unit expression by L4 gene products. *J Virol* **78**, 1782–1791.
188 Crisostomo L, Soriano AM, Mendez M, Graves D and Pelka P (2019) Temporal dynamics of adenovirus 5 gene expression in normal human cells. *PLoS ONE* **14**, e0211192.
189 Puvion-Dutilleul F and Puvion E (1991) Sites of transcription of adenovirus type 5 genomes in relation to early viral DNA replication in infected HeLa cells. A high resolution in situ hybridization and autoradiographical study. *Biol Cell* **71**, 135–147.
190 Puvion-Dutilleul F, Roussev R and Puvion E (1992) Distribution of viral RNA molecules during the adenovirus type 5 infectious cycle in HeLa cells. *J Struct Biol* **108**, 209–220.
191 Wu TC, Kanayama MD, Hruban RH, Au WC, Askin FB and Hutchins GM (1992) Virus-associated RNAs (VA-I and VA-II). An efficient target for the detection of adenovirus infections by in situ hybridization. *Am J Pathol* **140**, 991–998.
192 Jimenezgarcia L (1993) In vivo evidence that transcription and splicing are coordinated by a recruiting mechanism. *Cell* **73**, 47–59.
193 Zhang G, Taneja KL, Singer RH and Green MR (1994) Localization of pre-mRNA splicing in mammalian nuclei. *Nature* **372**, 809–812.
194 Bridge E and Pettersson U (1996) Nuclear organization of adenovirus RNA biogenesis. *Exp Cell Res* **229**, 233–239.
195 Gama-Carvalho M, Krauss RD, Chiang L, Valcárcel J, Green MR and Carmo-Fonseca M (1997) Targeting of U2AF^{65} to sites of active splicing in the nucleus. *J Cell Biol* **137**, 975–987.
196 Gama-Carvalho M (2003) Regulation of adenovirus alternative RNA splicing correlates with a reorganization of splicing factors in the nucleus. *Exp Cell Res* **289**, 77–85.
197 Custodio N (2004) In vivo recruitment of exon junction complex proteins to transcription sites in mammalian cell nuclei. *RNA* **10**, 622–633.
198 Krzywkowski T, Ciftci S, Assadian F, Nilsson M and Punga T (2017) Simultaneous single-cell *in situ* analysis of human adenovirus type 5 DNA and mRNA expression patterns in lytic and persistent infection. *J Virol* **91**, e00166-17.
199 Conze T, Göransson J, Razzaghian HR, Ericsson O, Oberg D, Akusjärvi G, Landegren U and Nilsson M (2010) Single molecule analysis of combinatorial splicing. *Nucleic Acids Res* **38**, e163.
200 Punga T, Ciftci S, Nilsson M and Krzywkowski T (2018) In situ detection of adenovirus DNA and mRNA in individual cells. *Curr Protoc Microbiol* **49**, e54.
201 Bann DV and Parent LJ (2012) Application of live-cell RNA imaging techniques to the study of retroviral RNA trafficking. *Viruses* **4**, 963–979.
202 Martin RM, Rino J, Carvalho C, Kirchhausen T and Carmo-Fonseca M (2013) Live-cell visualization of pre-mRNA splicing with single-molecule sensitivity. *Cell Rep* **4**, 1144–1155.
203 Riahi R, Dean Z, Wu T-H, Teitell MA, Chiou P-Y, Zhang DD and Wong PK (2013) Detection of mRNA in living cells by double-stranded locked nucleic acid probes. *Analyst* **138**, 4777–4785.
204 Wang F, Flanagan J, Su N, Wang L-C, Bui S, Nielson A, Wu X, Vo H-T, Ma X-J and Luo Y (2012) RNAscope: a novel in situ RNA analysis platform for formalin-fixed, paraffin-embedded tissues. *J Mol Diagn* **14**, 22–29.
205 Chen M, Ma Z, Wu X, Mao S, Yang Y, Tan J, Krueger CJ and Chen AK (2017) A molecular beacon-based approach for live-cell imaging of RNA transcripts with minimal target engineering at the single-molecule level. *Sci Rep* **7**, 1–11.
206 Volpi CC, Ciniselli CM, Gualeni AV, Plebani M, Alfieri S, Verderio P, Locati L, Perrone F, Quattrone P, Carbone A *et al*. (2018) In situ hybridization detection methods for HPV16 E6/E7 mRNA in identifying transcriptionally active HPV infection of oropharyngeal carcinoma: an updating. *Hum Pathol* **74**, 32–42.
207 Roe CJ, Siddiqui MT, Lawson D and Cohen C (2019) RNA in situ hybridization for Epstein-Barr virus and cytomegalovirus: comparison with in situ hybridization and immunohistochemistry. *Appl Immunohistochem Mol Morphol* **27**, 155–159.
208 Sandri-Goldin RM (2004) Viral regulation of mRNA export. *J Virol* **78**, 4389–4396.

209 Fontoura BM, Faria PA and Nussenzveig DR (2005) Viral interactions with the nuclear transport machinery: discovering and disrupting pathways. *IUBMB Life* **57**, 65–72.
210 Kuss SK, Mata MA, Zhang L and Fontoura BMA (2013) Nuclear imprisonment: viral strategies to arrest host mRNA nuclear export. *Viruses* **5**, 1824–1849.
211 Babiss LE, Ginsberg HS and Darnell JE (1985) Adenovirus E1B proteins are required for accumulation of late viral mRNA and for effects on cellular mRNA translation and transport. *Mol Cell Biol* **5**, 2552–2558.
212 Pilder S, Moore M, Logan J and Shenk T (1986) The adenovirus E1B–55K transforming polypeptide modulates transport or cytoplasmic stabilization of viral and host cell mRNAs. *Mol Cell Biol* **6**, 470–476.
213 Ornelles DA and Shenk T (1991) Localization of the adenovirus early region 1B 55-kilodalton protein during lytic infection: association with nuclear viral inclusions requires the early region 4 34-kilodalton protein. *J Virol* **65**, 424–429.
214 Dobbelstein M, Roth J, Kimberly WT, Levine AJ and Shenk T (1997) Nuclear export of the E1B 55-kDa and E4 34-kDa adenoviral oncoproteins mediated by a rev-like signal sequence. *EMBO J* **16**, 4276–4284.
215 Dosch T, Horn F, Schneider G, Krätzer F, Dobner T, Hauber J and Stauber RH (2001) The adenovirus type 5 E1B–55K oncoprotein actively shuttles in virus-infected cells, whereas transport of E4orf6 is mediated by a CRM1-independent mechanism. *J Virol* **75**, 5677–5683.
216 Rabino C, Aspegren A, Corbin-Lickfett K and Bridge E (2000) Adenovirus late gene expression does not require a Rev-like nuclear RNA export pathway. *J Virol* **74**, 6684–6688.
217 Carter CC, Izadpanah R and Bridge E (2003) Evaluating the role of CRM1-mediated export for adenovirus gene expression. *Virology* **315**, 224–233.
218 Yatherajam G, Huang W and Flint SJ (2011) Export of adenoviral late mRNA from the nucleus requires the Nxf1/Tap export receptor. *J Virol* **85**, 1429–1438.
219 Schmid M, Gonzalez RA and Dobner T (2012) CRM1-dependent transport supports cytoplasmic accumulation of adenoviral early transcripts. *J Virol* **86**, 2282–2292.
220 Shanmugam G, Bhaduri S, Arens M and Green M (1975) DNA binding proteins in the cytoplasm and in a nuclear membrane complex isolated from uninfected and adenovirus 2 infected cells. *Biochemistry* **14**, 332–337.
221 Kanellopoulos PN, van der Zandt H, Tsernoglou D, van der Vliet PC and Tucker PA (1995) Crystallization and preliminary X-ray crystallographic studies on the adenovirus ssDNA binding protein in complex with ssDNA. *J Struct Biol* **115**, 113–116.
222 Puvion-Dutilleul F and Puvion E (1990) Replicating single-stranded adenovirus type 5 DNA molecules accumulate within well-delimited intranuclear areas of lytically infected HeLa cells. *Eur J Cell Biol* **52**, 379–388.
223 Puvion-Dutilleul F and Puvion E (1990) Analysis by in situ hybridization and autoradiography of sites of replication and storage of single- and double-stranded adenovirus type 5 DNA in lytically infected HeLa cells. *J Struct Biol* **103**, 280–289.
224 Voelkerdingt K and Klessigt DF (1986) Identification of two nuclear subclasses of the adenovirus type 5-encoded DNA-binding protein. *J Virol* **60**, 10.
225 Deppert W, Walser A and Klockmann U (1988) A subclass of the adenovirus 72K DNA binding protein specifically associating with the cytoskeletal framework of the plasma membrane. *Virology* **165**, 457–468.
226 Cleghon V, Voelkerding K, Morin N, Delsert C and Klessig DF (1989) Isolation and characterization of a viable adenovirus mutant defective in nuclear transport of the DNA-binding protein. *J Virol* **63**, 2289–2299.
227 Morin N, Delsert C and Klessig DF (1989) Nuclear localization of the adenovirus DNA-binding protein: requirement for two signals and complementation during viral infection. *Mol Cell Biol* **9**, 4372–4380.
228 Garcés Y, Guerrero A, Hidalgo P, López RE, Wood CD, Gonzalez RA and Rendón-Mancha JM (2016) Automatic detection and measurement of viral replication compartments by ellipse adjustment. *Sci Rep* **6**, 36505.
229 Lee TWR, Lawrence FJ, Dauksaite V, Akusjärvi G, Blair GE and Matthews DA (2004) Precursor of human adenovirus core polypeptide Mu targets the nucleolus and modulates the expression of E2 proteins. *J Gen Virol* **85**, 185–196.
230 Lawrence FJ (2006) Nucleolar protein upstream binding factor is sequestered into adenovirus DNA replication centres during infection without affecting RNA polymerase I location or ablating rRNA synthesis. *J Cell Sci* **119**, 2621–2631.
231 Ching W, Koyuncu E, Singh S, Arbelo-Roman C, Hartl B, Kremmer E, Speiseder T, Meier C and Dobner T (2013) A ubiquitin-specific protease possesses a decisive role for adenovirus replication and oncogene-mediated transformation. *PLoS Pathog* **9**, e1003273.
232 Reyes ED, Kulej K, Pancholi NJ, Akhtar LN, Avgousti DC, Kim ET, Bricker DK, Spruce LA, Koniski SA, Seeholzer SH *et al.* (2017) Identifying host factors associated with DNA replicated during virus infection. *Mol Cell Proteomics* **16**, 2079–2097.
233 Doucas V, Ishov AM, Romo A, Juguilon H, Weitzman MD, Evans RM and Maul GG (1996) Adenovirus replication is coupled with the dynamic

properties of the PML nuclear structure. *Genes Dev* **10**, 196–207.
234 Kindsmüller K, Groitl P, Härtl B, Blanchette P, Hauber J and Dobner T (2007) Intranuclear targeting and nuclear export of the adenovirus E1B–55K protein are regulated by SUMO1 conjugation. *Proc Natl Acad Sci USA* **104**, 6684–6689.
235 Lam YW, Evans VC, Heesom KJ, Lamond AI and Matthews DA (2010) Proteomics analysis of the nucleolus in adenovirus-infected cells. *Mol Cell Proteomics* **9**, 117–130.
236 Genoveso MJ, Hisaoka M, Komatsu T, Wodrich H, Nagata K and Okuwaki M (2019) Formation of adenovirus DNA replication compartments and viral DNA accumulation sites by host chromatin regulatory proteins including NPM1. *FEBS J*. https://doi.org/10.1111/febs.15027.
237 Hidalgo P, Anzures L, Hernández-Mendoza A, Guerrero A, Wood CD, Valdés M, Dobner T and Gonzalez RA (2016) Morphological, biochemical, and functional study of viral replication compartments isolated from adenovirus-infected cells. *J Virol* **90**, 3411–3427.
238 Okuwaki M, Iwamatsu A, Tsujimoto M and Nagata K (2001) Identification of nucleophosmin/B23, an acidic nucleolar protein, as a stimulatory factor for in vitro replication of adenovirus DNA complexed with viral basic core proteins. *J Mol Biol* **311**, 41–55.
239 Matthews DA (2001) Adenovirus protein V induces redistribution of nucleolin and B23 from nucleolus to cytoplasm. *J Virol* **75**, 1031–1038.
240 Hindley CE, Davidson AD and Matthews DA (2007) Relationship between adenovirus DNA replication proteins and nucleolar proteins B23.1 and B23.2. *J Gen Virol* **88**, 3244–3248.
241 Samad MA, Komatsu T, Okuwaki M and Nagata K (2012) B23/nucleophosmin is involved in regulation of adenovirus chromatin structure at late infection stages, but not in virus replication and transcription. *J Gen Virol* **93**, 1328–1338.
242 Ugai H, Dobbins GC, Wang M, Le LP, Matthews DA and Curiel DT (2012) Adenoviral protein V promotes a process of viral assembly through nucleophosmin 1. *Virology* **432**, 283–295.
243 Ishibashi M and Maizel JV (1974) The polypeptides of adenovirus: V. Young virions, structural intermediate between top components and aged virions. *Virology* **57**, 409–424.
244 Morgan C, Godman GC, Rose HM, Howe C and Huang JS (1957) Electron microscopic and histochemical studies of an unusual crystalline protein occurring in cells infected by type 5 adenovirus. Preliminary observations. *J Biophys Biochem Cytol* **3**, 505–508.
245 Boulanger PA, Torpier G and Biserte G (1970) Investigation on intranuclear paracrystalline inclusions induced by adenovirus 5 in KB cells. *J Gen Virol* **6**, 329–332.
246 Marusyk R, Norrby E and Marusyk H (1972) The relationship of adenovirus-induced paracrystalline structures to the virus core protein(s). *J Gen Virol* **14**, 261–270.
247 Philipson L (1983) Structure and assembly of adenoviruses. In The Molecular Biology of Adenoviruses 1: 30 Years of Adenovirus Research 1953–1983 (Doerfler W, ed.), pp. 1–52. Springer Berlin Heidelberg, Berlin, Heidelberg.
248 Hasson TB, Soloway PD, Ornelles DA, Doerfler W and Shenk T (1989) Adenovirus L1 52- and 55-kilodalton proteins are required for assembly of virions. *J Virol* **63**, 3612–3621.
249 Hasson TB (1992) Adenovirus Li 52- and 55-kilodalton proteins are present within assembling virions and colocalize with nuclear structures distinct from replication centers. *J Virol* **66**, 10.
250 Weber JM, Déry CV, Mirza MA and Horvath J (1985) Adenovirus DNA synthesis is coupled to virus assembly. *Virology* **140**, 351–359.
251 Gustin KE, Lutz P and Imperiale MJ (1996) Interaction of the adenovirus L1 52/55-kilodalton protein with the IVa2 gene product during infection. *J Virol* **70**, 6463–6467.
252 Zhang W and Imperiale MJ (2000) Interaction of the adenovirus IVa2 protein with viral packaging sequences. *J Virol* **74**, 2687–2693.
253 Ostapchuk P, Anderson ME, Chandrasekhar S and Hearing P (2006) The L4 22-kilodalton protein plays a role in packaging of the adenovirus genome. *J Virol* **80**, 6973–6981.
254 Ostapchuk P, Almond M and Hearing P (2011) Characterization of empty adenovirus particles assembled in the absence of a functional adenovirus IVa2 protein. *J Virol* **85**, 5524–5531.
255 Ostapchuk P and Hearing P (2008) Adenovirus IVa2 protein binds ATP. *J Virol* **82**, 10290–10294.
256 Ahi YS, Vemula SV and Mittal SK (2013) Adenoviral E2 IVa2 protein interacts with L4 33K protein and E2 DNA-binding protein. *J Gen Virol* **94**, 1325–1334.
257 Ahi YS, Hassan AO, Vemula SV, Li K, Jiang W, Zhang GJ and Mittal SK (2017) Adenoviral E4 34K protein interacts with virus packaging components and may serve as the putative portal. *Sci Rep* **7**, 7582.
258 Ostapchuk P, Suomalainen M, Zheng Y, Boucke K, Greber UF and Hearing P (2017) The adenovirus major core protein VII is dispensable for virion assembly but is essential for lytic infection. *PLOS Pathog* **13**, e1006455.
259 Russell WC and Kemp GD (1995) Role of adenovirus structural components in the regulation of adenovirus infection. In The Molecular Repertoire of Adenoviruses I: Virion Structure and Infection

(Doerfler W and Böhm P, eds), pp. 81–98. Springer Berlin Heidelberg, Berlin, Heidelberg.
260 Matthews DA and Russell WC (1998) Adenovirus core protein V is delivered by the invading virus to the nucleus of the infected cell and later in infection is associated with nucleoli. *J Gen Virol* **79**, 1671–1675.
261 Scaria A, Tollefson AE, Saha SK and Wold WS (1992) The E3–11.6K protein of adenovirus is an Asn-glycosylated integral membrane protein that localizes to the nuclear membrane. *Virology* **191**, 743–753.
262 Rodriguez-Rocha H, Gomez-Gutierrez JG, Garcia-Garcia A, Rao X-M, Chen L, McMasters KM and Zhou HS (2011) Adenoviruses induce autophagy to promote virus replication and oncolysis. *Virology* **416**, 9–15.
263 Jiang H, White EJ, Ríos-Vicil CI, Xu J, Gomez-Manzano C and Fueyo J (2011) Human adenovirus type 5 induces cell lysis through autophagy and autophagy-triggered caspase activity. *J Virol* **85**, 4720–4729.
264 Unterholzner L (2013) The interferon response to intracellular DNA: why so many receptors? *Immunobiology* **218**, 1312–1321.
265 Ahtiainen L, Mirantes C, Jahkola T, Escutenaire S, Diaconu I, Österlund P, Kanerva A, Cerullo V and Hemminki A (2010) Defects in innate immunity render breast cancer initiating cells permissive to oncolytic adenovirus. *PLoS ONE* **5**, e13859.
266 Zhu J, Huang X and Yang Y (2007) Innate immune response to adenoviral vectors is mediated by both toll-like receptor-dependent and -independent pathways. *J Virol* **81**, 3170–3180.
267 Stein SC and Falck-Pedersen E (2012) Sensing adenovirus infection: activation of interferon regulatory factor 3 in RAW 264.7 cells. *J Virol* **86**, 4527–4537.
268 Lam E, Stein S and Falck-Pedersen E (2014) Adenovirus detection by the cGAS/STING/TBK1 DNA sensing cascade. *J Virol* **88**, 974–981.
269 Maler MD, Nielsen PJ, Stichling N, Cohen I, Ruzsics Z, Wood C, Engelhard P, Suomalainen M, Gyory I, Huber M *et al*. (2017) Key role of the scavenger receptor MARCO in mediating adenovirus infection and subsequent innate responses of macrophages. *mBio* **8**, e00670-17.
270 Mallery DL, McEwan WA, Bidgood SR, Towers GJ, Johnson CM and James LC (2010) Antibodies mediate intracellular immunity through tripartite motif-containing 21 (TRIM21). *Proc Natl Acad Sci USA* **107**, 19985–19990.
271 Bidgood SR, Tam JCH, McEwan WA, Mallery DL and James LC (2014) Translocalized IgA mediates neutralization and stimulates innate immunity inside infected cells. *Proc Natl Acad Sci USA* **111**, 13463–13468.
272 Watkinson RE, McEwan WA, Tam JCH, Vaysburd M and James LC (2015) TRIM21 promotes cGAS and RIG-I sensing of viral genomes during infection by antibody-opsonized virus. *PLoS Pathog* **11**, e1005253.
273 Barlan AU, Griffin TM, McGuire KA and Wiethoff CM (2011) Adenovirus membrane penetration activates the NLRP3 inflammasome. *J Virol* **85**, 146–155.
274 Smith JG and Nemerow GR (2008) Mechanism of adenovirus neutralization by human alpha-defensins. *Cell Host Microbe* **3**, 11–19.
275 Bottermann M, Foss S, Caddy SL, Clift D, van Tienen LM, Vaysburd M, Cruickshank J, O'Connell K, Clark J, Mayes K *et al*. (2019) Complement C4 prevents viral infection through capsid inactivation. *Cell Host Microbe* **25**, 617–629.e7.
276 Everett RD (2001) DNA viruses and viral proteins that interact with PML nuclear bodies. *Oncogene* **20**, 7266–7273.
277 Geoffroy M-C and Chelbi-Alix MK (2011) Role of promyelocytic leukemia protein in host antiviral defense. *J Interferon Cytokine Res* **31**, 145–158.
278 Schreiner S and Wodrich H (2013) Virion factors that target Daxx to overcome intrinsic immunity. *J Virol* **87**, 10412–10422.
279 Scherer M and Stamminger T (2016) Emerging role of PML nuclear bodies in innate immune signaling. *J Virol* **90**, 5850–5854.
280 Komatsu T, Nagata K and Wodrich H (2016) An adenovirus DNA replication factor, but not incoming genome complexes, targets PML nuclear bodies. *J Virol* **90**, 1657–1667.
281 Komatsu T, Will H, Nagata K and Wodrich H (2016) Imaging analysis of nuclear antiviral factors through direct detection of incoming adenovirus genome complexes. *Biochem Biophys Res Commun* **473**, 200–205.
282 Ishov AM and Maul GG (1996) The periphery of nuclear domain 10 (ND10) as site of DNA virus deposition. *J Cell Biol* **134**, 815–826.
283 Carvalho T, Seeler JS, Ohman K, Jordan P, Pettersson U, Akusjärvi G, Carmo-Fonseca M and Dejean A (1995) Targeting of adenovirus E1A and E4-ORF3 proteins to nuclear matrix-associated PML bodies. *J Cell Biol* **131**, 45–56.
284 Puvion-Dutilleul F, Venturini L, Guillemin MC, de Thé H and Puvion E (1995) Sequestration of PML and Sp100 proteins in an intranuclear viral structure during herpes simplex virus type 1 infection. *Exp Cell Res* **221**, 448–461.
285 Ou HD, Kwiatkowski W, Deerinck TJ, Noske A, Blain KY, Land HS, Soria C, Powers CJ, May AP, Shu X *et al*. (2012) A structural basis for the assembly and functions of a viral polymer that inactivates multiple tumor suppressors. *Cell* **151**, 304–319.

286 Leppard KN and Everett RD (1999) The adenovirus type 5 E1b 55K and E4 Orf3 proteins associate in infected cells and affect ND10 components. *J Gen Virol* **80** (Pt 4), 997–1008.
287 Ullman AJ and Hearing P (2008) Cellular proteins PML and Daxx mediate an innate antiviral defense antagonized by the adenovirus E4 ORF3 protein. *J Virol* **82**, 7325–7335.
288 Rosa-Calatrava M, Puvion-Dutilleul F, Lutz P, Dreyer D, de Thé H, Chatton B and Kedinger C (2003) Adenovirus protein IX sequesters host-cell promyelocytic leukaemia protein and contributes to efficient viral proliferation. *EMBO Rep* **4**, 969–975.
289 Schreiner S, Martinez R, Groitl P, Rayne F, Vaillant R, Wimmer P, Bossis G, Sternsdorf T, Marcinowski L, Ruzsics Z *et al*. (2012) Transcriptional activation of the adenoviral genome is mediated by capsid protein VI. *PLoS Pathog* **8**, e1002549.
290 Stracker TH, Carson CT and Weitzman MD (2002) Adenovirus oncoproteins inactivate the Mre11-Rad50-NBS1 DNA repair complex. *Nature* **418**, 348–352.
291 Evans JD and Hearing P (2005) Relocalization of the Mre11-Rad50-Nbs1 complex by the adenovirus E4 ORF3 protein is required for viral replication. *J Virol* **79**, 6207–6215.
292 Stracker TH, Lee DV, Carson CT, Araujo FD, Ornelles DA and Weitzman MD (2005) Serotype-specific reorganization of the Mre11 complex by adenoviral E4orf3 proteins. *J Virol* **79**, 6664–6673.
293 Harada JN, Shevchenko A, Shevchenko A, Pallas DC and Berk AJ (2002) Analysis of the adenovirus E1B–55K-anchored proteome reveals its link to ubiquitination machinery. *J Virol* **76**, 9194–9206.
294 Querido E, Blanchette P, Yan Q, Kamura T, Morrison M, Boivin D, Kaelin WG, Conaway RC, Conaway JW and Branton PE (2001) Degradation of p53 by adenovirus E4orf6 and E1B55K proteins occurs via a novel mechanism involving a Cullin-containing complex. *Genes Dev* **15**, 3104–3117.
295 Schwartz RA, Lakdawala SS, Eshleman HD, Russell MR, Carson CT and Weitzman MD (2008) Distinct requirements of adenovirus E1b55K protein for degradation of cellular substrates. *J Virol* **82**, 9043–9055.
296 Karen KA and Hearing P (2011) Adenovirus core protein VII protects the viral genome from a DNA damage response at early times after infection. *J Virol* **85**, 4135–4142.
297 Shah GA and O'Shea CC (2015) Viral and cellular genomes activate distinct DNA damage responses. *Cell* **162**, 987–1002.
298 Avgousti DC, Fera AND, Otter CJ, Herrmann C, Pancholi NJ and Weitzman MD (2017) Adenovirus core protein VII downregulates the DNA damage response on the host genome. *J Virol* **91**, e01089-17.
299 Leonard GT and Sen GC (1996) Effects of adenovirus E1A protein on interferon-signaling. *Virology* **224**, 25–33.
300 Sohn S-Y and Hearing P (2011) Adenovirus sequesters phosphorylated STAT1 at viral replication centers and inhibits STAT dephosphorylation. *J Virol* **85**, 7555–7562.
301 Morgan C, Godman GC, Breitenfeld PM and Rose HM (1960) A correlative study by electron and light microscopy of the development of type 5 adenovirus. I. Electron microscopy. *J Exp Med* **112**, 373–382.
302 Jun S, Ke D, Debiec K, Zhao G, Meng X, Ambrose Z, Gibson GA, Watkins SC and Zhang P (1993) Direct visualization of HIV-1 with correlative live-cell microscopy and cryo-electron tomography. *Structure* **19**, 1573–1581.
303 Welsch S, Miller S, Romero-Brey I, Merz A, Bleck CKE, Walther P, Fuller SD, Antony C, Krijnse-Locker J and Bartenschlager R (2009) Composition and three-dimensional architecture of the dengue virus replication and assembly sites. *Cell Host Microbe* **5**, 365–375.
304 Sharma M, Kamil JP, Coughlin M, Reim NI and Coen DM (2014) Human cytomegalovirus UL50 and UL53 recruit viral protein kinase UL97, not protein kinase C, for disruption of nuclear lamina and nuclear egress in infected cells. *J Virol* **88**, 249–262.
305 Bykov YS, Cortese M, Briggs JAG and Bartenschlager R (2016) Correlative light and electron microscopy methods for the study of virus-cell interactions. *FEBS Lett* **590**, 1877–1895.
306 Ou HD, Deerinck TJ, Bushong E, Ellisman MH and O'Shea CC (2015) Visualizing viral protein structures in cells using genetic probes for correlated light and electron microscopy. *Methods* **90**, 39–48.
307 Schellenberger P, Kaufmann R, Siebert CA, Hagen C, Wodrich H and Grünewald K (2014) High-precision correlative fluorescence and electron cryo microscopy using two independent alignment markers. *Ultramicroscopy* **143**, 41–51.
308 Riedel C, Vasishtan D, Siebert CA, Whittle C, Lehmann MJ, Mothes W and Grünewald K (2017) Native structure of a retroviral envelope protein and its conformational change upon interaction with the target cell. *J Struct Biol* **197**, 172–180.
309 Hagen C, Dent KC, Zeev-Ben-Mordehai T, Grange M, Bosse JB, Whittle C, Klupp BG, Siebert CA, Vasishtan D, Bäuerlein FJB *et al*. (2015) Structural basis of vesicle formation at the inner nuclear membrane. *Cell* **163**, 1692–1701.
310 Carl D, Kemper B, Wernicke G and von Bally G (2004) Parameter-optimized digital holographic microscope for high-resolution living-cell analysis. *Appl Opt* **43**, 6536–6544.
311 Yakimovich A, Witte R, Andriasyan V, Georgi F and Greber UF (2018) Label-free digital holo-tomographic

microscopy reveals virus-induced cytopathic effects in live cells. *mSphere* **3**, e00599-18.
312 Snijder J, Reddy VS, May ER, Roos WH, Nemerow GR and Wuite GJL (2013) Integrin and defensin modulate the mechanical properties of adenovirus. *J Virol* **87**, 2756–2766.
313 Ortega-Esteban A, Pérez-Berná AJ, Menéndez-Conejero R, Flint SJ, Martín CS and de Pablo PJ (2013) Monitoring dynamics of human adenovirus disassembly induced by mechanical fatigue. *Sci Rep* **3**, 1434.
314 Ortega-Esteban A, Condezo GN, Pérez-Berná AJ, Chillón M, Flint SJ, Reguera D, San Martín C and de Pablo PJ (2015) Mechanics of viral chromatin reveals the pressurization of human adenovirus. *ACS Nano* **9**, 10826–10833.
315 Keller PJ and Stelzer EHK (2010) Digital scanned laser light sheet fluorescence microscopy. *Cold Spring Harb Protoc* **2010**, pdb.top78.
316 Strobl F, Schmitz A and Stelzer EHK (2017) Improving your four-dimensional image: traveling through a decade of light-sheet-based fluorescence microscopy research. *Nat Protoc* **12**, 1103–1109.
317 Christiansen EM, Yang SJ, Ando DM, Javaherian A, Skibinski G, Lipnick S, Mount E, O'Neil A, Shah K, Lee AK *et al*. (2018) In silico labeling: predicting fluorescent labels in unlabeled images. *Cell* **173**, 792–803.e19.
318 Ounkomol C, Seshamani S, Maleckar MM, Collman F and Johnson GR (2018) Label-free prediction of three-dimensional fluorescence images from transmitted-light microscopy. *Nat Methods* **15**, 917–920.
319 von Chamier L, Laine RF and Henriques R (2019) Artificial intelligence for microscopy: what you should know. *Biochem Soc Trans* **47**, 1029–1040.
320 Andriasyan V, Yakimovich A, Georgi F, Petkidis A, Witte R, Puntener D and Greber UF (2019) Deep learning of virus infections reveals mechanics of lytic cells. *bioRxiv* 798074 [PREPRINT].
321 Russell WC, Patel G, Precious B, Sharp I and Gardner PS (1981) Monoclonal antibodies against adenovirus type 5: preparation and preliminary characterization. *J Gen Virol* **56**, 393–408.
322 Cepko CL, Changelian PS and Sharp PA (1981) Immunoprecipitation with two-dimensional pools as a hybridoma screening technique: production and characterization of monoclonal antibodies against adenovirus 2 proteins. *Virology* **110**, 385–401.
323 Boudin ML, D'Halluin JC, Cousin C and Boulanger P (1980) Human adenovirus type 2 protein IIIa. II. Maturation and encapsidation. *Virology* **101**, 144–156.
324 Lunt R, Vayda ME, Young M and Flint SJ (1988) Isolation and characterization of monoclonal antibodies against the adenovirus core proteins. *Virology* **164**, 275–279.
325 Balakirev MY, Jaquinod M, Haas AL and Chroboczek J (2002) Deubiquitinating function of adenovirus proteinase. *J Virol* **76**, 6323–6331.
326 Lutz P and Kedinger C (1996) Properties of the adenovirus IVa2 gene product, an effector of late-phase-dependent activation of the major late promoter. *J Virol* **70**, 1396–1405.
327 Reich NC, Sarnow P, Duprey E and Levine AJ (1983) Monoclonal antibodies which recognize native and denatured forms of the adenovirus DNA-binding protein. *Virology* **128**, 480–484.
328 Webster A, Leith IR and Hay RT (1997) Domain organization of the adenovirus preterminal protein. *J Virol* **71**, 539–547.
329 White E, Spector D and Welch W (1988) Differential distribution of the adenovirus E1A proteins and colocalization of E1A with the 70-kilodalton cellular heat shock protein in infected cells. *J Virol* **62**, 4153–4166.
330 Spindler KR, Rosser DS and Berk AJ (1984) Analysis of adenovirus transforming proteins from early regions 1A and 1B with antisera to inducible fusion antigens produced in *Escherichia coli*. *J Virol* **49**, 132–141.
331 Harlow E, Franza BR and Schley C (1985) Monoclonal antibodies specific for adenovirus early region 1A proteins: extensive heterogeneity in early region 1A products. *J Virol* **55**, 533–546.
332 Lucher LA, Kimelman D, Symington JS, Brackmann KH, Cartas MA, Thornton H and Green M (1984) Identification of adenovirus 12-encoded E1A tumor antigens synthesized in infected and transformed mammalian cells and in *Escherichia coli*. *J Virol* **52**, 136–144.
333 Murti KG, Davis DS and Kitchingman GR (1990) Localization of adenovirus-encoded DNA replication proteins in the nucleus by immunogold electron microscopy. *J Gen Virol* **71** (Pt 12), 2847–2857.
334 Friefeld BR, Korn R, de Jong PJ, Sninsky JJ and Horwitz MS (1985) The 140-kDa adenovirus DNA polymerase is recognized by antibodies to *Escherichia coli*-synthesized determinants predicted from an open reading frame on the adenovirus genome. *Proc Natl Acad Sci USA* **82**, 2652–2656.
335 Tollefson AE, Scaria A, Saha SK and Wold WS (1992) The 11,600-MW protein encoded by region E3 of adenovirus is expressed early but is greatly amplified at late stages of infection. *J Virol* **66**, 3633–3642.
336 Boivin D, Morrison MR, Marcellus RC, Querido E and Branton PE (1999) Analysis of Synthesis, stability, phosphorylation, and interacting polypeptides of the 34-kilodalton product of open reading frame 6 of the early region 4 protein of human adenovirus type 5. *J Virol* **73**, 1245–1253.
337 Nevels M, Täuber B, Kremmer E, Spruss T, Wolf H and Dobner T (1999) Transforming potential of the adenovirus type 5 E4orf3 protein. *J Virol* **73**, 1591–1600.